AD-635219

STUDIES AND EXPERIMENTAL WORK ON ATOMIC COLLISION PROCESSES OCCURRING IN ATMOSPHERIC GASES

A. V. Phelps and W. H. Kasner

Westinghouse Research Laboratories
Pittsburgh, Pennsylvania

Contract AF29(601)-6729

TECHNICAL REPORT NO. AFWL-TR-66-34

May 1966

AIR FORCE WEAPONS LABORATORY
Research and Technology Division
Air Force Systems Command
Kirtland Air Force Base
New Mexico

DDC

RECEIVED

JUL 18 1966

D

AFWL-TR-66-34

Research and Technology Division
AIR FORCE WEAPONS LABORATORY
Air Force Systems Command
Kirtland Air Force Base
New Mexico

DISCLAIMER NOTICE

THIS DOCUMENT IS BEST QUALITY PRACTICABLE. THE COPY FURNISHED TO DTIC CONTAINED A SIGNIFICANT NUMBER OF PAGES WHICH DO NOT REPRODUCE LEGIBLY.

STUDIES AND EXPERIMENTAL WORK ON ATOMIC COLLISION
PROCESSES OCCURRING IN ATMOSPHERIC GASES

A. V. Phelps and W. H. Kasner

Westinghouse Research Laboratories
Pittsburgh, Pennsylvania
Contract AF29(601)-6729

TECHNICAL REPORT NO. AFWL-TR-66-34

FOREWORD
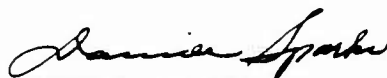
This report was prepared by the Westinghouse Research Laboratories, Pittsburgh, Pennsylvania, under Contract AF29(601)-6729. The research was performed under Program Element 7.60.06.01.D, Project 5710, Subtask 07.010, and was funded by the Defense Atomic Support Agency (DASA).

Inclusive dates of research were 22 December 1964 to 22 December 1965. The report was submitted 10 March 1966 by the AFWL Project Officer, Capt David C. Sparks (WLRTH). The report carries the corporate designation: Research Report 66-6E2-GASES-R1, Westinghouse Proprietary Class 3.

The work discussed in the various sections of this report was carried out by the following personnel: Section III, W. H. Kasner; Section IV, J. L. Moruzzi and A. V. Phelps; Section V, A. V. Phelps and R. D. Hake, Jr.

Previous work under this series of contracts is summarized in Technical Report AFWL-TR-64-178.

This report has been reviewed and is approved.

DAVID C. SPARKS
Captain   USAF
Project Officer

RALPH H. PENNINGTON
Colonel   USAF
Chief, Theoretical Branch

WILLIAM H. STEPHENS
Colonel   USAF
Chief, Research Division

ii

ABSTRACT

Temperature dependent recombination studies in nitrogen have been conducted over the range 200–480°K, yielding a coefficient of $(2.9 \pm 0.3) \times 10^{-7} \text{cm}^3/\text{sec}$ for the recombination of N_2^+ ions and electrons. The observed temperature dependence is quite small, being adequately described by the relation $T^{-0.02}$. Several modifications have been made on the flow system used in the study of associative detachment in O_2-O mixtures. In subsequent studies a reaction resembling associative detachment has been observed. While preliminary tests were being conducted on the rf mass spectrometer which is to be used on the flow system, a brief study of negative ion-molecule reactions was made. Rate coefficients for several of these reactions were measured. A summary of the results of a calculation of momentum transfer and inelastic cross sections for electrons in oxygen is presented. The computed momentum transfer cross section is in satisfactory agreement with electron beam results but it differs significantly from the cross section obtained at thermal energies from microwave experiments.

(This page was intentionally left blank)

TABLE OF CONTENTS

(This page was intentionally left blank)

STUDIES AND EXPERIMENTAL WORK ON ATOMIC COLLISION
PROCESSES OCCURRING IN ATMOSPHERIC GASES

I

INTRODUCTION

The work discussed in this report is part of a general program of
laboratory measurements of some of the important rates of electron inter-
action with atmospheric gases. Such information is useful for prediction and
analysis of the electrical properties of the earth's atmosphere resulting
from ionizing radiation. The portion of this work supported by the Air Force
Weapons Laboratory is directed toward a more accurate determination of the
rates of electron depletion and production in air as a result of electron
attachment and detachment and electron-ion recombination, and toward an improve-
ment in our ability to predict the behavior of these electrons in the presence
of electric fields. The period of the research covered by this report is 22
December 1964 through 22 December 1965.

SUMMARY

The objectives of the research program described in this technical report have been: a) initiate an experimental investigation of the temperature dependence of electron-positive ion recombination in atmospheric gases; b) continue experimental studies of electron attachment and detachment in mixtures of atomic and molecular oxygen; and c) improve our ability to predict the behavior of electrons in air by improving our determination of a set of elastic and inelastic scattering cross sections for electrons in oxygen.

The experimental techniques and the results of the temperature dependent recombination studies in atmospheric gases, primarily nitrogen, are presented in Section III. The recombination studies in nitrogen have been conducted over the temperature range 200 to 480°K yielding a recombination coefficient for N_2^+ ions and electrons in agreement with our published value,[1] $\alpha (N_2^+) = (2.9 \pm 0.3) \times 10^{-7} cm^3/sec$. The observed temperature dependence is quite small, being adequately described by the relation $T^{-0.02}$. The observed recombination coefficients exhibited no systematic dependence on the pressures of the gases (N_2 and Ne) used in the experiments so long as N_2^+ was the only significant afterglow positive ion, thus indicating that the observed recombination reaction is a two-body process involving only N_2^+ ions and electrons. The present results are in strong disagreement with other published works[2] which claim temperature dependences of from T^{-1} to $T^{-3/2}$ in the case of nitrogen. One is not really justified in making a comparison with these previous observations since the recombining positive ion species have not been identified in these cases. Our own observations[3] seem to indicate that the more complex ions N_3^+ and N_4^+ may have been the predominant ion species in these previously reported results. Attempts to study the temperature dependent recombination of N_3^+, or N_4^+, ions with electrons have thus far been unsuccessful, since we have been unable to obtain afterglow conditions where only one of the ion species dominates.

In preparation for a study of electron-ion recombination in oxygen, the microwave system was modified for single pulse operation. Subsequent recombination studies in N_2-Ne mixtures, at room temperature, have yielded results in agreement with our previous measurements. In addition, using the single pulse technique, we have found afterglow conditions where N_4^+ is the only

positive ion species detected. Thus far we have not conducted any temperature dependent recombination studies using this single pulse technique.

Section IV describes the experiments wh.ch have been performed in the study of electron attachment in O_2-0 mixtures. A flow system capable of producing a mixture of atomic and molecular oxygen, as well as oxygen negative ions, has been built. By a suitable choice of electric field strength in the negative ion source either O_2^- or O^- can be formed. Discharge noise and electrostatic charging have been reduced to satisfactory levels by the use of an aluminum flow tube in the ion reaction region rather than the conventional glass flow tube. On initiating a discharge, an apparent destruction of the negative ions has been observed suggesting a detachment mechanism involving the negative ions and the neutral products of the discharge. It is not yet known whether the apparent detachment is due to associative detachment or to some other process.

While carring out various tests on the mass spectrometer to be used with the flow tube for negative ion mass identification, we have made a brief study of some negative ion-molecule reactions. In pure oxygen at low E/p we observe only O_2^- ions which are formed by a three-body attachment process. We also find that at E/p > 1 $Vcm^{-1}Torr^{-1}$ three negative ions, O^-, O_2^- and O_3^- are formed. The mechanisms involved in their production are 1) dissociative attachment, 2) charge transfer, and 3) three-body ion-molecule reaction, respectively. The rate coefficient for the production of O_3^- from O^- was found to be 1.5 x $10^{-31} cm^6 sec^{-1}$. Measurements with carbon dioxide indicate that O^- is formed at E/p > 7 V $cm^{-1}Torr^{-1}$ by a dissociative attachment mechanism. This reaction is then followed by a very rapid conversion to CO_3^- via a three-body ion-molecule reaction. In mixtures of CO_2 and O_2 one observes the production of O_2^- by a three-body attachment process at low values of E/p. This O_2^- undergoes conversion by a three-body reaction to produce CO_4^-. The rate coefficients for the formation of these complex CO_3^- and CO_4^- ions from O^- and O_2^- are estimated to be 1.3 x 10^{-28} and 1.28 x 10^{-29} $cm^6 sec^{-1}$, respectively. In water vapor at E/p > 10 $Vcm^{-1}Torr^{-1}$, the ions H^-, OH^- and $(H_2O)_n \cdot OH^-$, (where n = 1,2,3,4,5) are observed. It is thought that H^- is the initial ion produced. It subsequently reacts with H_2O to form OH^-. Clustering of OH^- with various numbers of water molecules then occurs. If oxygen is added to the water vapor then, at low E/p, O_2^- is initially formed. The clustering of O_2^- with water then produces $(H_2O)_n \cdot O_2^-$ where n = 1,2,3,4. The situation in water

3

and water mixtures is very complex and should be investigated further. No complex ions are observed in mixtures of nitrogen and oxygen.

Section V of this report summarizes the results of our determinations of momentum transfer and inelastic cross sections for electrons in oxygen. Our results are based on an analysis of measured drift velocities and characteristic energies for electrons in the presence of a dc electric field. The results are expected to be most accurate in the range of electron energies in which vibrational excitation is the dominant energy loss mechanism. It appears that the assumption which is most consistent with all of the available experimental data is that the vibrational excitation cross section consists of a series of sharp resonances centered about the vibrational states of the O_2^- ion. The magnitudes of the integrals of the resonance cross sections are approximately 10^{-18} cm^2 eV. We have obtained estimates of inelastic cross sections with excitation thresholds at 4.5, 8.0, and 9.7 eV. The momentum transfer or elastic scattering cross section obtained from this analysis is in satisfactory agreement with electron beam results, but it differs significantly from the cross section obtained at thermal energies from microwave experiments. Until this discrepancy is resolved, we cannot make truly accurate predictions of radio propagation characteristics in air.

III

ELECTRON-ION RECOMBINATION STUDIES IN ATMOSPHERIC GASES

III A. Introduction

Large two-body electron-ion recombination rates have been measured in laboratory studies of ionized gas afterglows[4] and inferred from the analysis of observations of the ionospheric regions of the upper atmosphere.[5] In noble gas (e.g., neon, argon, krypton and xenon) afterglows the observed thermal ($\sim 300^{\circ}$K) recombination coefficients have been found to be in the 10^{-7} - 10^{-6} cm^3/sec range. Under the conditions of these experiments the diatomic molecular ions are expected to be the predominant positive ion species; thus, dissociative recombination

$$X_2^+ + e \; \rightleftarrows \; (X_2^*)_{unstable} \; \rightleftarrows \; X^* + X + \text{kinetic energy} \tag{1}$$
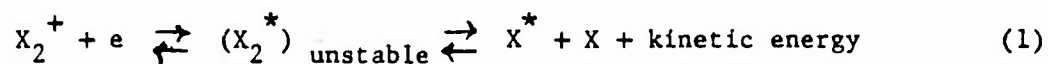
where the superscripts + and * represent ionized and excited states, respec- tively, is the probable electron capture process.

In recent years there has been considerable interest in the recombination of low energy electrons with ions of the type found in the ionosphere; thus, studies of electron-ion recombination in atmospheric gases are desirable. At the present time, techniques of theoretical analysis are not sufficiently advanced to yield reliable quantitative calculations of the dissociative recombination rates for particular atmospheric ions; therefore, appeal has been made to laboratory measurements of the desired rates. Mass spectrometric observations[3] have shown that it is difficult to prevent the formation of polyatomic ions such as N_3^+, N_4^+ and O_3^+ in these atmospheric gas studies. As a consequence, many of the previous recombination studies do not apply to the ion assumed to be present (e.g., N_2^+ or O_2^+), leading to considerable confusion in the literature.[6]

This section of the report contains a description of the techniques and the results of our temperature dependent studies of electron-positive ion recombination in atmospheric gases. During the present contract our efforts have been devoted primarily to the study of recombination in nitrogen. In subsections III B and III C are presented brief descriptions of the apparatus and the experimental techniques which are used in these investigations. The

results of the observations are presented in subsection III D. Subsection III E contains a description of the modified experimental techniques which are to be used in the temperature dependent recombination study of oxygen.

III B. Apparatus

In the study of volume recombination by microwave techniques, the essential experimental measurement is the determination of the free electron density in a cavity as a function of time after cessation of a discharge. The electron density is obtained by measuring the shift of the resonant frequency of the cavity due to the presence of the electron gas.[7,8] This experimental technique is adequately described in the literature; hence, we shall only outline our basic procedures.

The microwave system is shown schematically in Fig. 1. The discharge is initiated in the cavity (resonant at ∿3000 Mc/sec) by a pulse from the magnetron. The duration of the discharge can be varied over the range 25 μsec to 2.5 msec. Following the discharge pulse a very low power probing signal from the klystron is incident on the cavity. The signal reflected from the cavity is detected by the crystal, passed through a non-overloading amplifier and displayed on an oscilloscope. After a short time interval, 10-20 msec, the magnetron is switched on again and the cycle is repeated.

The frequency of the klystron is swept, i.e., increased with time during the afterglow,[8] thereby "sharpening" the absorption dips in the late afterglow where the electron density is changing more slowly. The frequency measurement range of the microwave system provides reliable measures of the electron density between 2×10^{10} and 1×10^{7} electrons/cm^3.

Figure 2 shows a simplified sketch of the microwave cavity and the associated apparatus. The cavity, shown in dark outline, is in the shape of a rectangular parallelepiped and is constructed of stainless steel. It is iris coupled to the 3000 Mc/sec microwave system discussed above.

Centered in the cavity wall opposite the coupling iris is a small (≈0.006 in. diameter) effusion orifice. Some of the afterglow ions which diffuse to the walls pass through this orifice and are focused onto an rf mass spectrometer[9] by a two-element ion lens, consisting of a mesh wire cylinder followed by a plane grid (not shown in Fig. 2). This lens is designed so that the electric field has a minimum value in the region near the
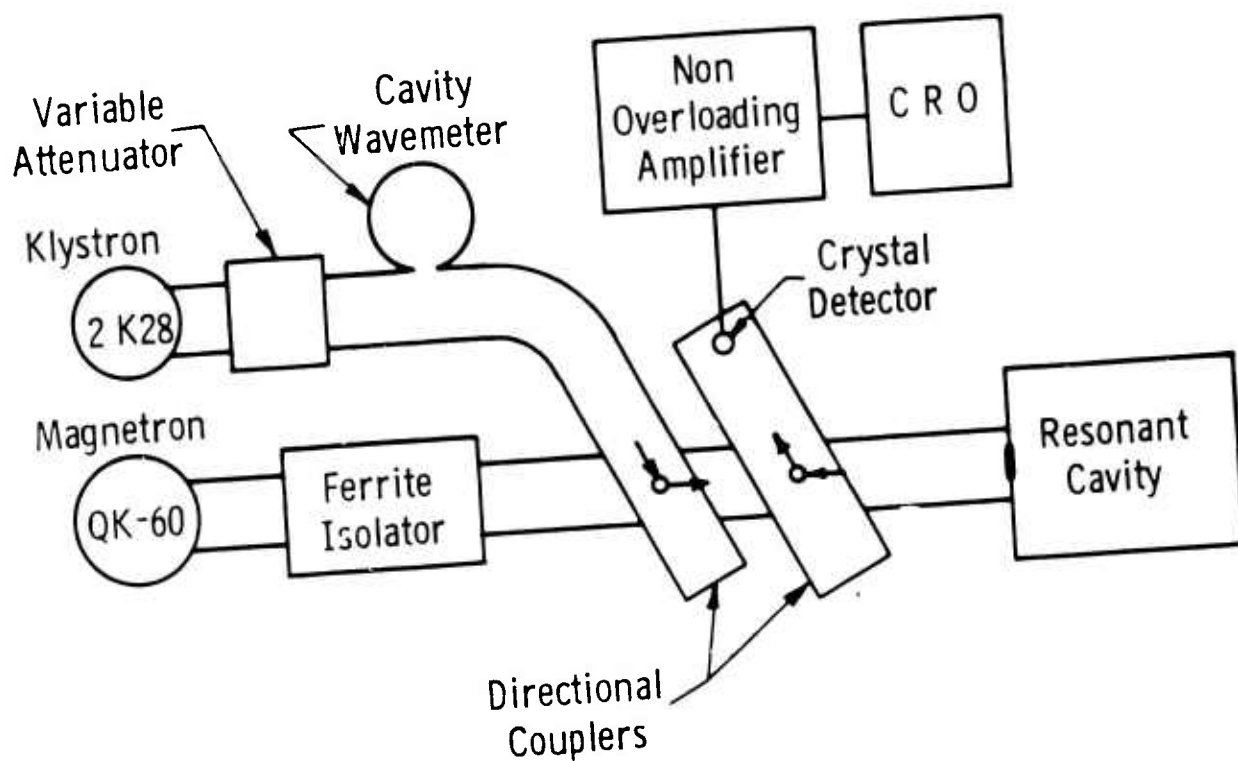
6

Fig. 1 Block diagram of the microwave system used to ionize the gas and measure the electron density during the afterglow.
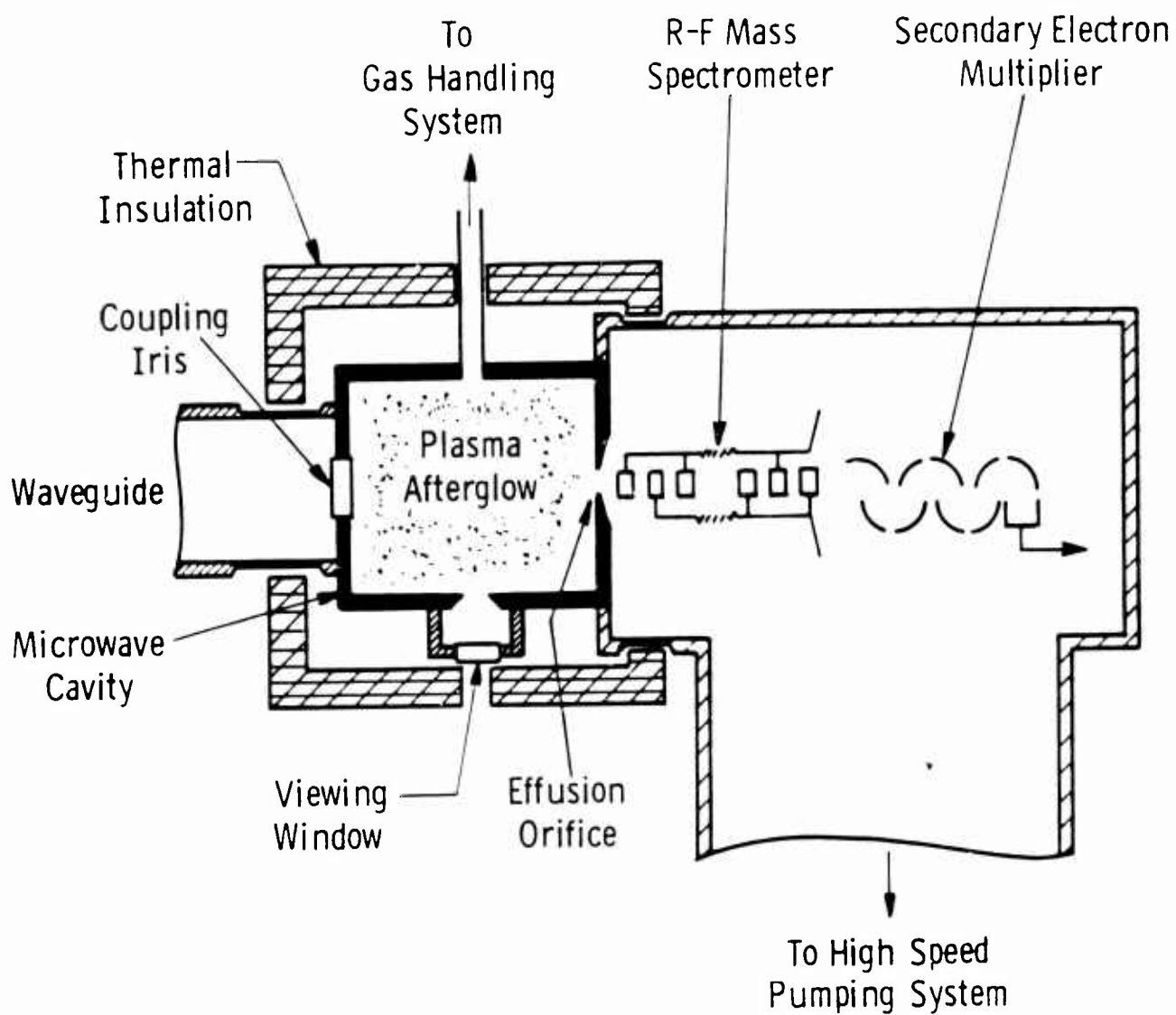
Fig. 2 Simplified sketch of the microwave cavity and rf mass
spectrometer.

orifice where the gas pressure is high, thereby reducing the probability of ion conversion reactions resulting from collisions between the accelerating ions and the neutral gas.

The neutral gas which flows through the orifice passes readily through the open mesh wire lens elements and is pumped away by a high speed (100 liter/sec) pumping system consisting of an oil diffusion pump and a zeolite isolation trap.[10] Typically the pressure in the rf mass spectrometer chamber is less than 10^{-3} Torr for cavity pressures up to 20 Torr.

The entire vacuum system consisting of the cavity, the rf mass spectrometer, the gas handling system, and the zeolite traps can be baked at temperatures up to 400°C to reduce the impurity level. At room temperature the resulting background pressures are consistently less than 10^{-8} Torr in all parts of the system.

In the high temperature recombination studies the cavity is heated by a small "clam shell" electric furnace (not shown in Fig. 2). The heat losses from the cavity are minimized by the thermal insulation and by the thin-walled stainless steel sections located in the waveguide section and in the rf mass spectrometer housing. For the low temperature studies, dry ice was packed around a heavy copper cylinder which, in turn, was in good thermal contact with the flanges at both ends of the cavity. The cavity temperature was monitored by several thermocouples attached to it at various points. The temperature was always uniform throughout the cavity to within a few degrees.

III C. Experimental Procedures. Nitrogen Recombination Study

In general the decay rate of an afterglow plasma is dependent on various competing reaction, i.e., diffusion, ion conversion, electron attachment, etc., as well as the electron-ion recombination reaction which we wish to study. In order to make a simple interpretation of the afterglow decay in terms of electron-ion recombination, it is necessary to minimize these competing reactions. If one further assumes that the afterglow is dominated by a single positive ion species, then the electron continuity equation becomes simply,

$$\frac{dn_e}{dt} = - \alpha\, n_e n_+ \qquad (2)$$

9

where α is the recombination coefficient and n_e and n_+ are the electron and positive ion densities, respectively. On the assumption of quasineutrality of the plasma and negligible negative ion concentration. i.e., $n_+ \cong n_e$ Eq. (2) becomes,

$$\frac{dn_e}{dt} = - \alpha \, n_e^2 \qquad (3)$$

with the well known "recombination solution,"

$$1/n_e = [1/n_e(0)] + \alpha \, t . \qquad (4)$$

The experimental results presented in this report were analyzed on the basis of this simple relation.

The first step in the recombination studies is to insure that the afterglows are dominated by a single ion species whose identity has been established. Preliminary studies[3] have shown that the ions N^+ to N_4^+ can be present in the afterglow of a nitrogen discharge. The relative concentrations of these ions depends on the experimental conditions, i.e., the gas pressure and the discharge power level and pulse length. However, the parent molecular ion, N_2^+, is the dominant afterglow ion species if the nitrogen pressure is kept below approximately 10^{-3} Torr, the exact upper limit being a function of the cavity temperature, T_c. Since the microwave system will not operate properly at such low pressures, it has been necessary to mix in inert buffer gases in order to achieve these experimental conditions. Neon has been used as the buffer gas for all the observations reported here.

The other experimental techniques which have been used in these investigations to minimize the significant competing reactions have been discussed in detail in the literature[1] and presented in the last final report (AFWL-TR-64-178); hence, they do not need to be restated here.

During the early stages of the temperature dependent recombination studies in N_2-Ne gas mixtures, it was observed that significant concentrations of impurity ions in the mass 16 to 18 range appeared in the afterglow mass spectra when the cavity temperature exceeded $\approx 100^{\circ}C$. It was presumed that these ions represented water vapor and its fragments which were given off by the glass components of the cavity, i.e., the microwave coupling iris and the

viewing window. These components were finally replaced with sapphire ones with no significant decrease in the impurity level. We were, however, able to reduce the impurities to an acceptable level by first baking the cavity at temperatures 50 to 75°C above the desired operating temperature for extended periods of time, 48 to 72 hours. This technique was used successfully for operating temperatures up to approximately 500°K. Low temperature observations were also undertaken in an effort to further extend the temperature range of these recombination studies.

Some modifications of the system which might permit extension of the useful temperature range to 600°K have been considered. These modifications include: a) plating the inside of the cavity with a metal which would reduce the desorption of impurities and b) increase the gas flow rate through the cavity thus reducing the equilibrium impurity concentration.

III D. Results of Nitrogen Recombination Studies

An example of the experimental data obtained in the temperature dependent study of electron-ion recombination in nitrogen is shown in Fig. 3. Here we have plotted the reciprocals of the electron density and the N_2^+ ion wall current (the rf mass spectrometer output) as functions of time in the afterglow. In this case the N_2^+ ion wall currents have been normalized to the electron density at an afterglow time of 3 msec. One notes first of all that the electron density decay indicates recombination control during the entire afterglow, i.e., $1/n_e$ increases linearly with time as predicted by Eq. (4). The measured slope of this straight line is closely related to the desired recombination coefficient, α.

Figure 3 also shows that over the major part of the afterglow the N_2^+ ion wall current decay follows the electrons. This behavior, which implies that the electron and ion spatial distributions within the cavity do not change radically with time, is observed only under "good" recombination conditions.[1] We feel that the similarity in the temporal behavior of the electron density and the ion wall currents in recombination studies is important; for if this similar behavior exists, one can say, with some degree of confidence, that there are no significant reactions which preferentially deplete either the electrons or the positive ions. Furthermore, one can say that there are not likely to be any significant concentrations of
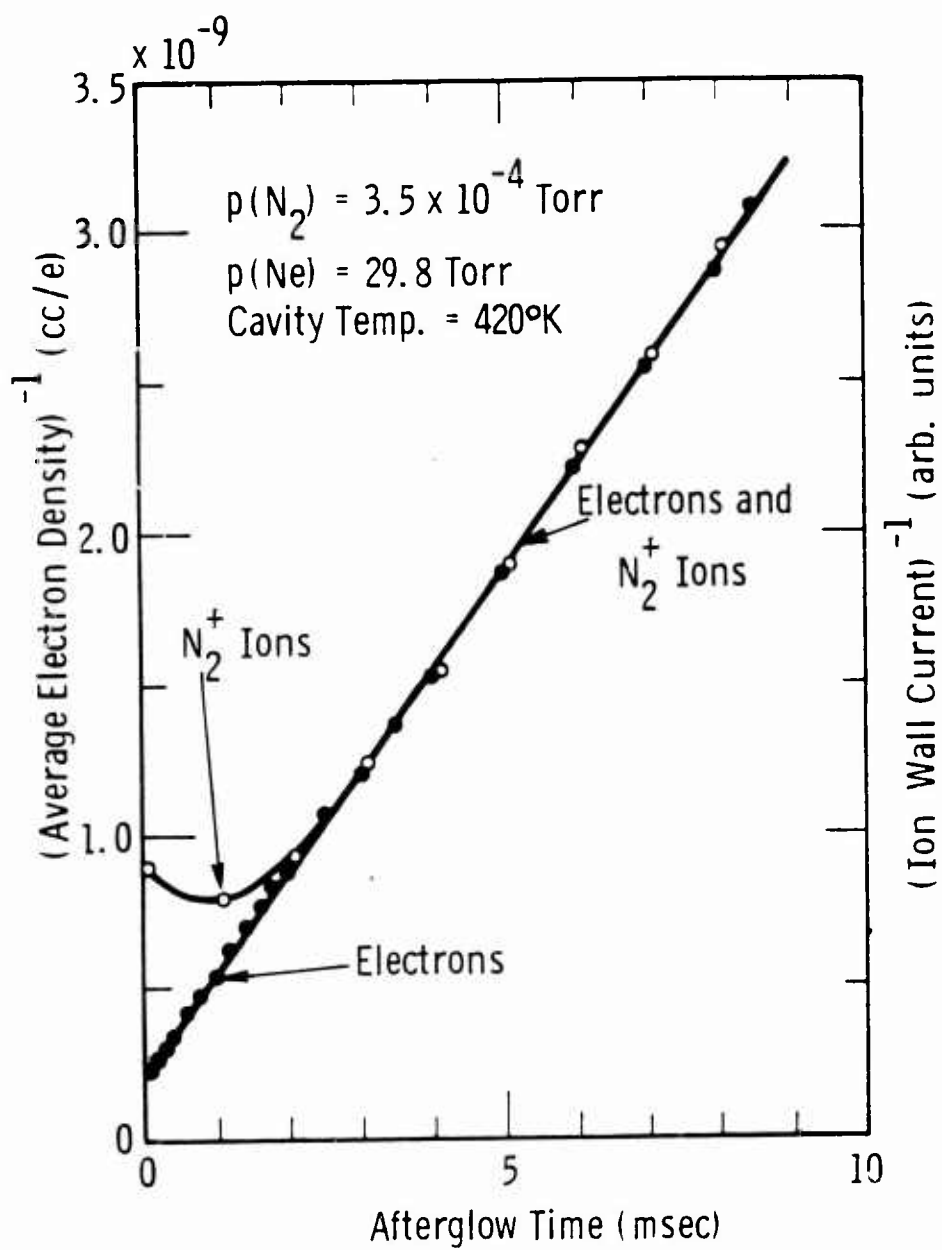
11

Fig. 3 Reciprocal electron density and N_2^+ ion wall currents as functions of time in the afterglow.

undetected ion species. This last point is particularly significant in cases where negative ions are likely to be present; for example, in the study of oxygen or nitric oxide.

Studies of the electron-ion recombination rates in N_2-Ne gas mixtures were conducted over a range of gas pressures. Figure 4 shows a plot of the observed recombination coefficients as a function of the neon pressure for a series of nitrogen pressures, all data corresponding to a cavity temperature of 378°K. One notes that within experimental error there is no dependence on either the nitrogen or neon gas pressure. A similar behavior is observed at all temperatures so long as the conditions for N_2^+ domination of the afterglow are satisfied. Thus, we conclude that the recombination reaction under study is a two-body process involving only N_2^+ ions and electrons.

Reliable temperature dependent recombination measurements in the N_2-Ne mixtures have been conducted over the temperature range 200 to 480°K. These results are presented in Fig. 5. The solid points in Fig. 5 represent the averages of several measurements made at each temperature, for a range of nitrogen and neon pressures. The vertical lines through the points show the standard deviations of these experimental values. One notes that there is very little temperature dependence in the observed recombination coefficients. The dotted line corresponds to our previously published[1] room temperature ($\approx 300^\circ$K) value, $\alpha (N_2^+) = (2.9 \pm 0.3) \times 10^{-7} cm^3$/sec. The solid line, which gives a reasonable fit to the data, has a temperature dependence of only $T^{-0.02}$. The overall confidence limit for the absolute values of the measured recombination coefficients is about $\pm 10\%$. The relative variation of the observed recombination coefficients as a function of temperature should be much more accurate than this since essentially the same systematic errors are present at each temperature.

Several measurements of the temperature dependence of electron-ion recombination in nitrogen have been reported in the literature.[2] In these cases temperature variations of the order of T^{-1} to $T^{-3/2}$ have been observed. In general, these measurements were conducted at gas pressures where our observations[3] show that N_3^+ and N_4^+ should be the predominant ion species; consequently, no comparison can be made with the present results. Recently we conducted some afterglow studies in N_2-Ne mixtures under conditions where the ion species N_2^+, N_3^+, and N_4^+ were all present. It was observed that the
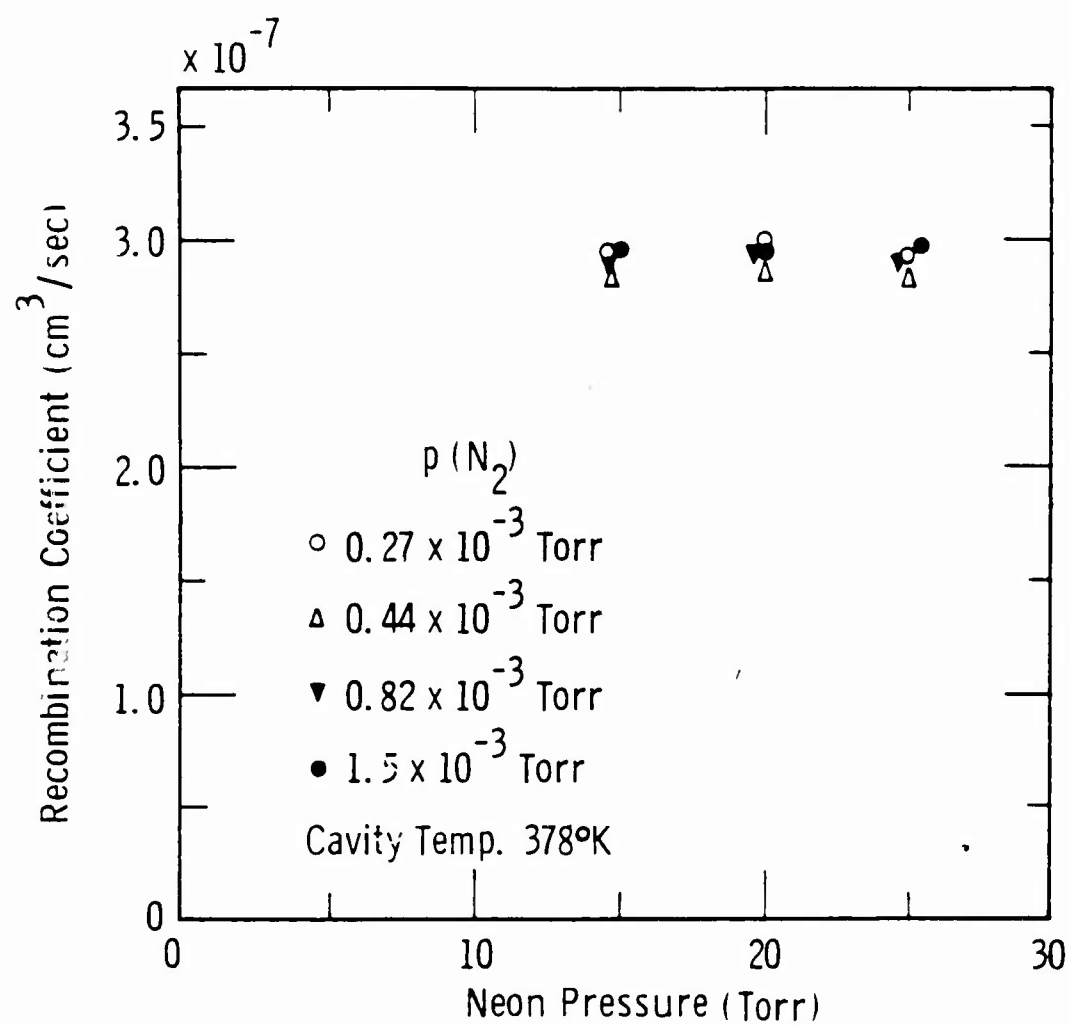
13

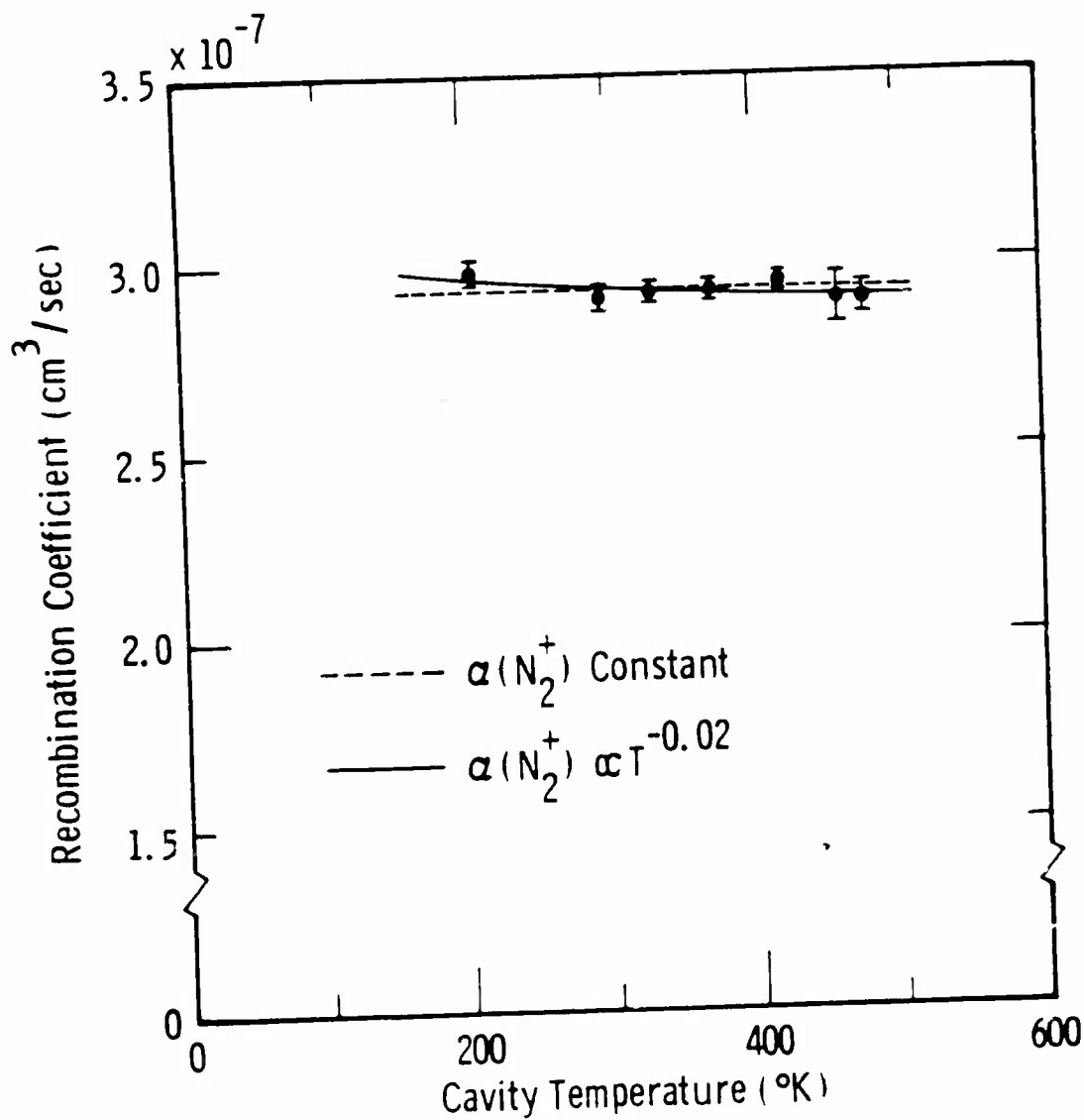Fig. 4 Nitrogen and neon pressure dependences of the observed
recombination coefficients.

14

Fig. 5 Temperature dependence of observed recombination
coefficients.

concentrations of the complex ions N_3^+ and N_4^+ relative to N_2^+ decreased by more than an order of magnitude as the gas temperature was increased from 300 to $500^\circ K$, the nitrogen and neon gas densities being maintained at constant values. If one extends these measurements to the pressure regime of the previously reported recombination studies, it is conceivable that a part of the observed temperature dependence may be due to changes in the relative concentration of the positive ion species. Without the benefit of mass analysis, it is extremely difficult to assess the significance of this contribution to the observed temperature dependence in the previous measurements. Within the last few weeks we have conducted some temperature dependent afterglow studies in N_2-Ne mixtures under conditions where N_3^+ and N_4^+ are the dominant ion species. We were unable to find a set of experimental conditions, i.e., gas pressures, discharge pulse lengths, etc., for which either N_3^+ or N_4^+ was the dominant afterglow ion species over the entire temperature range; hence, a measurement of the temperature dependent recombination coefficients for these ion species could not be made.

III E. System Modification for Oxygen Recombination Study

In subsection III C some modifications of the system which might permit extension of the useful temperature range were proposed. Before making these changes, we decided to investigate the temperature dependent electron-ion recombination in oxygen over the temperature range which is presently accessible. In the last final report (AFWL-TR-64-178), it was indicated that negative ions may have been responsible for the discrepancies observed in our previous afterglow recombination studies in O_2-Ne mixtures. The primary discrepancies were: a) different temporal decay rates for the electrons and positive ions and b) a dependence of the observed recombination coefficient on the duration of the afterglow for fixed discharge conditions. These observations seem to be consistent with a negative ion concentration which requires several cycles in order to reach its equilibrium value. Therefore, in the present oxygen recombination studies, we are initiating the single pulse mode of operation in order to reduce the negative ion effects to a minimum.

The basic operation of the microwave system in the single pulse mode is the same as in the cycled, or recurrent, mode except that the

16

magnetron is pulsed only once and, at present, the klystron frequency is fixed rather than being swept. For each pulse the crystal output observed on the oscilloscope is recorded photographically. The time dependence of the resonant frequency of the cavity during the afterglow period is determined from a sequence of single pulses each corresponding to a different fixed frequency of the klystron.

In the recurrent mode of operation there are usually a sufficient number of free electrons remaining in the cavity at the end of the afterglow period to provide consistent initiation of the next discharge when the magnetron is switched on. This is not the case in the single pulse mode of operation. Observations have indicated that the time intervals between the application of magnetron power and the initiation of the discharge in the cavity may be as long as 1 msec. Consistent firing of the discharge at the beginning of the magnetron pulse has been achieved by creating a small d.c. discharge between two pointed tungsten wires located in the plane of the cavity wall on the side containing the viewing window (see Fig. 2). This voltage pulse, which is coincident with the beginning of the magnetron pulse, is approximately 1 Kv in magnitude and 50 μsec in duration. A series ballast resistor is used to minimize sputtering and the subsequent release of impurities into the cavity.

After the change-over had been completed, it seemed advisable to check out the system by making some further studies of N_2-Ne gas mixtures. This work is underway at the present time. We have found that the room temperature recombination coefficient for N_2^+ ions and electrons is essentially in agreement, within 4%, with the value obtained via the recurrent mode of operation. Thus far we have made no temperature dependent studies using the single pulse mode of operation.

Another very interesting observation has resulted from these single pulse studies of N_2-Ne gas mixtures; in particular, as the nitrogen pressure is increased the dominant ion species becomes N_4^+. No N_3^+ is observed. Comparison mass spectra for the recurrent and single pulse modes are shown in Fig. 6. These mass spectra correspond to the same experimental conditions, i.e, gas pressures, discharge power level and pulse length. The mass spectra were obtained by frequency scanning of the rf mass spectrometer. In the recurrent mode of operation this gives a smooth trace as shown in the upper part of Fig. 6. In the single pulse mode of operation the mass scan

17
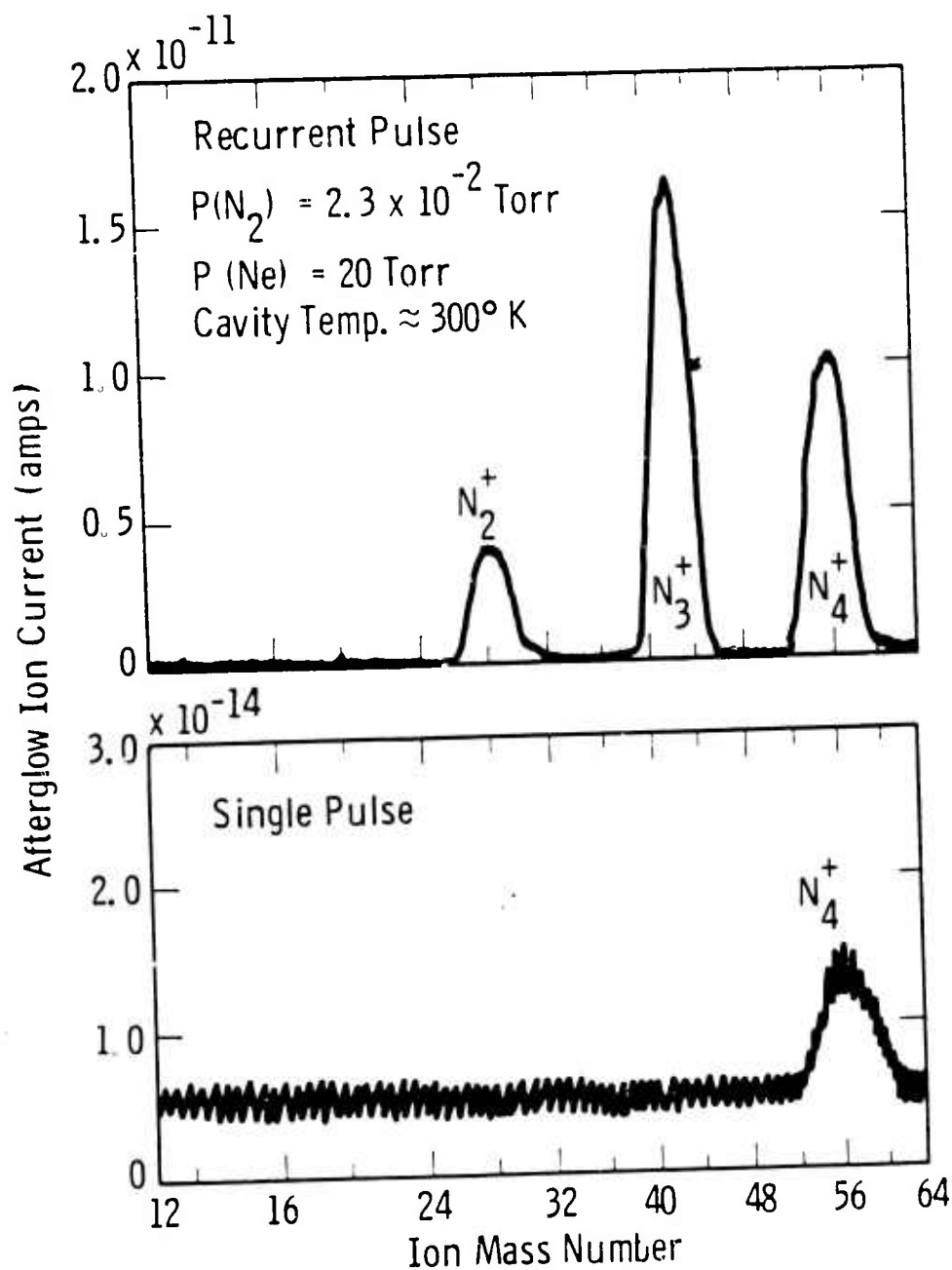
Fig. 6   Sample mass scans in the afterglow of a nitrogen-neon microwave discharge. These data correspond to time interval 1.0 to 1.2 msec after the termination of the discharge pulse.

18

consists of a series of current spikes corresponding to the individual pulses of the system. The "noisy" line drawn in the lower portion of Fig. 6 represents the envelope of these pulses.

At the present time we do not have a completely satisfactory explanation for the observed differences in these mass spectra. It has been suggested that the N_3^+ ions are formed via the reaction

$$N_4^+ + N \rightarrow N_3^+ + N_2. \tag{5}$$

The failure to observe N_3^+ in the single pulse mode then implies that many pulses are required in order to build the N atom density up to its recurrent mode equilibrium value. Further investigation is required in order to substantiate this hypothesis. In any case, it appears that the single pulse mode of operation offers the opportunity to study the temperature dependent recombination of N_4^+ ions and electrons.

ELECTRON ATTACHMENT AND DETACHMENT IN O_2-O MIXTURES

IV A. Introduction

The object of this experiment is to study electron attachment and detachment in the gases resulting from the dissociation of molecular oxygen, i.e., in mixtures of O, O_2, O_2^* and O_3.

We believe that in spite of the difficulties inherent in working with reactive species such as O and O_3, it is essential to have an understanding of the role of such species in determining the rates to electron depletion in the ambient and disturbed ionosphere. For example, it has been proposed by Bates and Massey[11] and others that the process of associative detachment [see Eq. (6) below] is responsible for observed electron detachment in the altitude range at which there is significant atomic oxygen. As yet, there is no laboratory evidence as to the rate of this process, so that one must rely on very crude theoretical estimates. At lower altitudes, the concentration of O_3 becomes appreciable and could result in a significant increase in the rate of electron attachment or in the formation of O_3^- ions which may be stable with regard to both collisional detachment and photodetachment.

Our first objective is to determine whether the rate of the reaction

$$O_2^- + O \rightarrow O_3 + e \tag{6}$$

can be measured in the laboratory. To the best of our knowledge, this is the first attempt to produce and study ions in dissociated gases at moderately high pressures (1 - 10 Torr); thus, many preliminary experiments have been necessary to become familiar with new techniques. At these pressures atomic oxygen can be produced by: a) the dissociation of molecular oxygen by a high microwave field; b) the dissociation of molecular nitrogen by a high microwave field and then adding an equimolar amount of nitric oxide; and c) the thermal decomposition of ozone.

In the past year method a) has been employed since it is somewhat more convenient, but the side production of excited molecular oxygen and ozone will limit its usefulness when accurate estimates of reaction (6) are made.

In future experiments method b) will be used to produce the atomic oxygen since O_2^* is eliminated when this technique is used.

The production of O_2^- at these pressures presents no serious problems, although the production of O_2^- at sufficiently high densities for the observation of detachment signals requires the use of a hot filament which can be operated for a reasonable length of time in oxygen. In these studies, thoriated iridium has been used as the filament material and life-times of up to 10 hours achieved. Attempts to improve the lifetime by using a high emission photocathode were unsuccessful since very rapid poisoning of the surface occurs when the oxygen discharge is initiated.

In order to ascertain the exact species of ions and neutrals reacting in the system, it is necessary to perform a mass analysis of both the ions and neutral particles. This requires a mass spectrometer capable of probing high pressure systems. An instrument capable of examining the ionic content of the system has been built and tested on an auxiliary system. The mass spectrometer chosen for this task is a Boyd[9] linear accelerator rf mass spectrometer. This instrument requires no magnets, a small power supply and operates at high pressures with very modest pumping requirements. In the process of building and testing the mass spectrometer some useful data on the negative ion mass spectrum of O_2, CO_2, H_2O as well as O_2-N_2, O_2-CO_2 and O_2-H_2 mixtures were obtained. Also the rates of several negative ion-molecule reactions of possible interest to ionospheric studies were determined. We plan to install this mass spectrometer on the flow system in the near future.

IV B. The Flow System

(IV B.1) Description of the Flow Tube

The flow tube is similar to that described in the previous report[12] except that the glass tube containing the electron gun and detachment regions of the system has been replaced by a length of aluminum tube. This tube is contained within a stainless steel envelope and is insulated from it by two Teflon collars (see Fig. 7). The electrodes in the detachment region are supported from the aluminum tube by Teflon inserts which also electrically isolate these electrodes from the aluminum tube. External connections to these electrodes are made through ceramic feedthroughs in
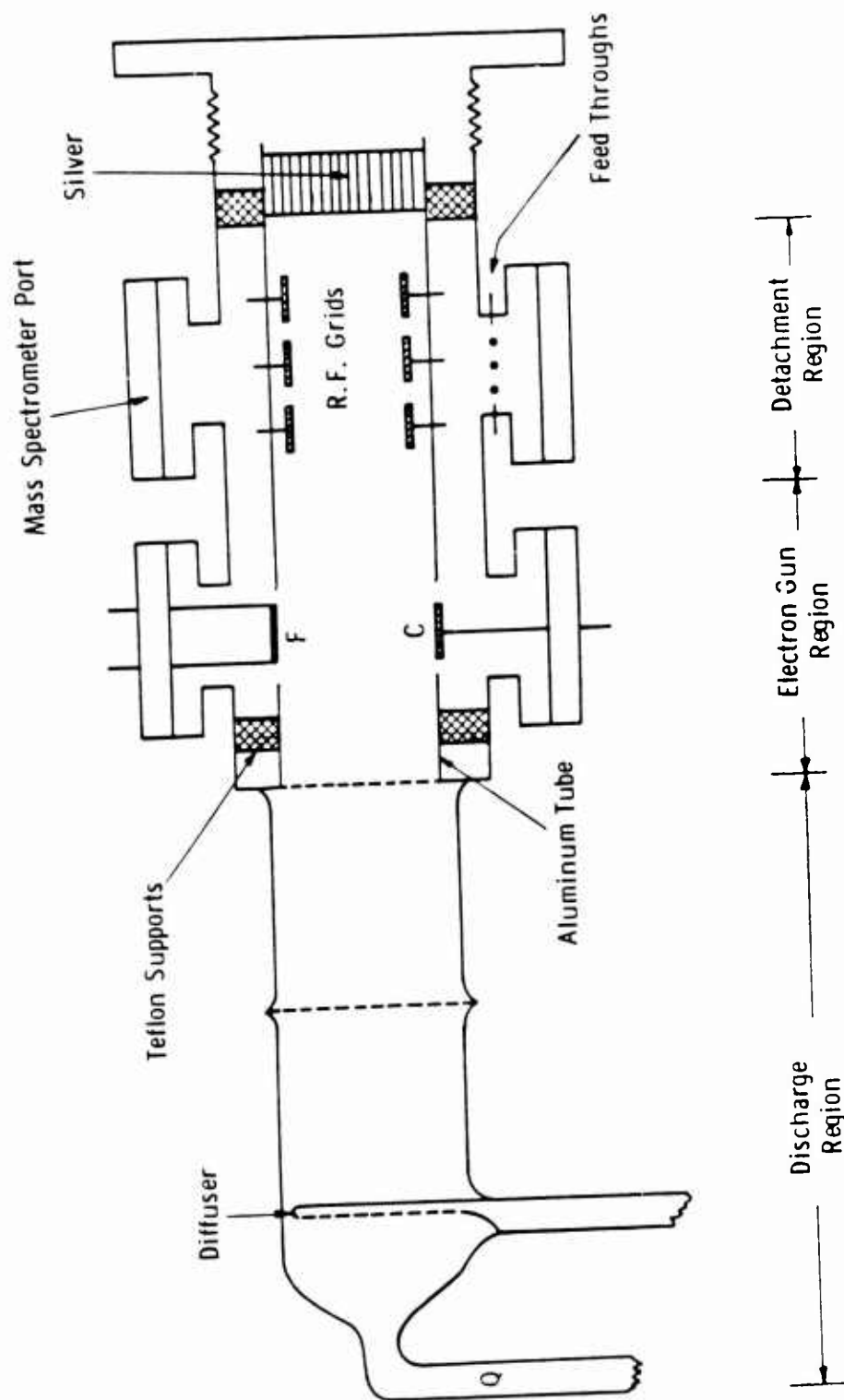
21

Fig. 7 Schematic diagram of the flow tube.

22

the stainless steel envelope. Provision to examine the light producing
reactions (to be described later) has been made by installing six small
sapphire windows at suitable positions along the stainless steel tube which
are in line with six 1/8" holes in the aluminum tube.

Extra dry grade oxygen, 99.6% pure, and commercial grade nitrogen
dioxide, 99.5% pure, were used throughout these experiments with no further
purification attempted. However, a glass bead filled liquid nitrogen trap
was installed in the oxygen line to be used at a later date when purified
oxygen will be required. Gases are admitted to the system through
Granville-Phillips variable leaks and the flow rates of either gas are
measured on specially calibrated flow meters. In general, flow velocities
between 200 and 400 cm/sec and pressures of 1 to 7 Torr are used.

Low energy electrons are produced by a hot thoriated iridium
filament, F, mounted on an easily demountable flange which mates with a
suitable flange on the stainless steel tube. Two 1-1/4" holes in the alum-
inum tube allow electrons to be pulled across the gas stream by an externally
applied electric field. Although the lifetimes of such filaments operating
in high oxygen pressures are short, it is still the most convenient
technique available. Attempts to use a high emission photo surface, of the
type described in subsection (IV C.1), were unsuccessful since on initiating
the discharge rapid poisoning of the photo surface occurs. The electrons
are drawn across the tube by a variable 20 Kc square wave voltage applied
between the filament F and collector C. This technique ensures that a good
fraction of the negative ions formed in the gas are swept downstream into the
detachment regions.

In the detachment region there are three pairs of plane electrodes
mounted parallel to each other, see Fig. 7, the outer electrodes eliminating
end effects for the center pair. To each pair of electrodes an rf or dc
voltage can be applied and the current collected by any pair of electrodes
is measured on a vibrating reed electrometer. The rf voltage for each pair
of electrodes is obtained from separate sources that can be varied from
0-700 volts over a frequency range of 50 Kc/sec to 2.0 Mc/sec. A typical
circuit for the electron gun and detachment regions can be seen in Fig. 8.
After the detachment region there is a 3" long silver honey-comb inserted
within the tube. This honey-comb does not appreciably restrict the gas
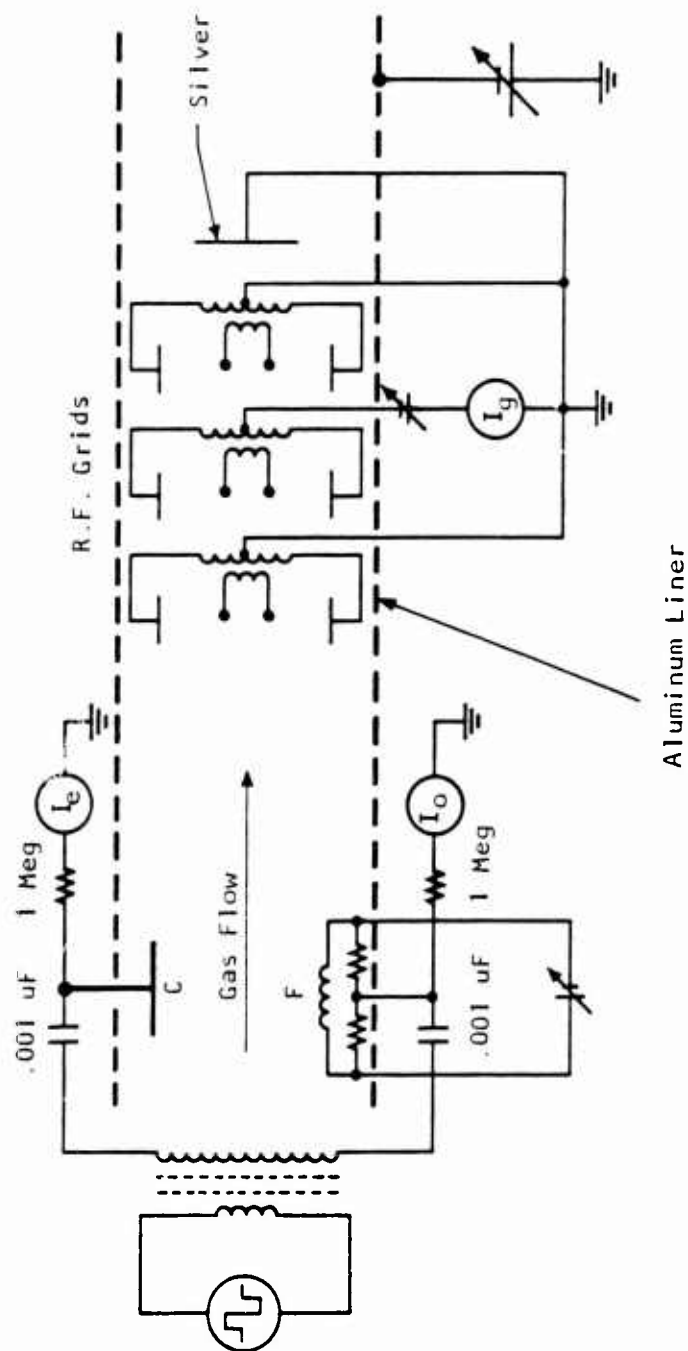flow but does destroy all surviving atomic oxygen before it can enter the

23

Fig. 8 Typical electron gun and detachment region circuit.

24

pumping line.

In order to determine the absolute atomic oxygen density at a given point along the flow tube and its subsequent decay along the tube, it is necessary to be able to measure the light output from the reactions represented by Eqs. (7) and (8) (to be presented shortly). Measurements of this light output were made using a 931 photomultiplier which was mounted on a platform that could be mechanically driven along the length of the flow tube. Photographic black cloth draped over the tube was sufficient to reduce the background light to a suitably low level.

A length of 13 mm O.D. quartz tubing admits oxygen to one end of the flow tube. This quartz tubing passes through a high power microwave field where partial dissociation of the gas flowing in the tube occurs. The microwave power is obtained from a QK-390 magnetron and associated equipment. For every given pressure in the main tube, the standing wave ratio in the wave guide was optimized by means of a stub tuner, and the power output of the magnetron was controlled by adjustments to its power supplies.

(IV B.2) Production of Atomic Oxygen

There are three techniques available for producing atomic oxygen at the pressures required for this experiment, and they have been described previously.[12] In the past year only one technique, the dissociation of molecular oxygen, has been used. The procedure followed in this technique is to admit oxygen to the system through the variable leak in the oxygen line until the required flow tube pressure is obtained, usually between 1 and 7 Torr. The magnetron is then switched on and a discharge initiated in the quartz section of the flow tube with a Tesla Coil. The stub tuner in the wave guide assembly is then adjusted until a satisfactory VSWR is obtained. Once this has been done the discharge is normally stable for long periods of time. The microwave powered discharge partially dissociates the oxygen and the resulting O_2-O mixture flows along the tube in the direction of the pumps.

The presence of impurities in the oxygen entering the discharge, e.g., H_2O, N_2, can cause a considerable increase in the production rate of atomic oxygen, but this condition is undesirable due to the more rapid decay

of O along the tube and other complicating effects. The disadvantage of
this technique for the production of atomic oxygen lies in the formation
of undesirable side products in the discharge, the principal ones being
ozone and excited states of oxygen, O_2^*. Evidence has been found[13] that
glass wool effectively removes excited states produced in a nitrogen dis-
charge but unfortunately this technique does not remove the excited
states produced in an oxygen discharge.

The temperature of the gas also has to be determined since, if
it is above $100^\circ C$, collisional detachment can occur.[14] Attempts to measure
this quantity are being made but no conclusions have as yet been reached.

To reduce the discharge noise in the detachment region a 5"
section of the 2" glass flow tube prior to the metal flow tube section has
been coated with aluminum and is maintained at a potential of -10 volts.

(IV B.3)   Measurement of the Atomic Oxygen Flow Rate

The flow rate of atomic oxygen, and hence its concentration, can
be determined by the "NO_2 titration" technique developed by Kaufmann.[15]
This technique requires the addition of a known amount of NO_2 to the O_2-O
mixture causing a bright yellow-green afterglow to be produced along the
tube by the following reactions,

$$NO_2 + O \rightarrow NO + O_2 \tag{7}$$

and

$$NO + O \rightarrow NO_2 + h\nu \tag{8}$$

As the amount of NO_2 added is increased, the intensity of the afterglow
initially increases, goes through a maximum and finally drops to zero as
reaction (7) consumes all of the atomic oxygen present. Thus, the NO_2
flow rate for maximum light output should be half that required to
extinguish the afterglow and this flow rate will be equivalent to half of
the atomic oxygen flow rate. A plot of afterglow intensity vs NO_2 flow
rate is presented in Fig. 9. These types of curves have not been as
satisfactory with the glass-aluminum flow tube as they were with the
initial all-glass system. It is felt that the NO_2 inlet is too close to
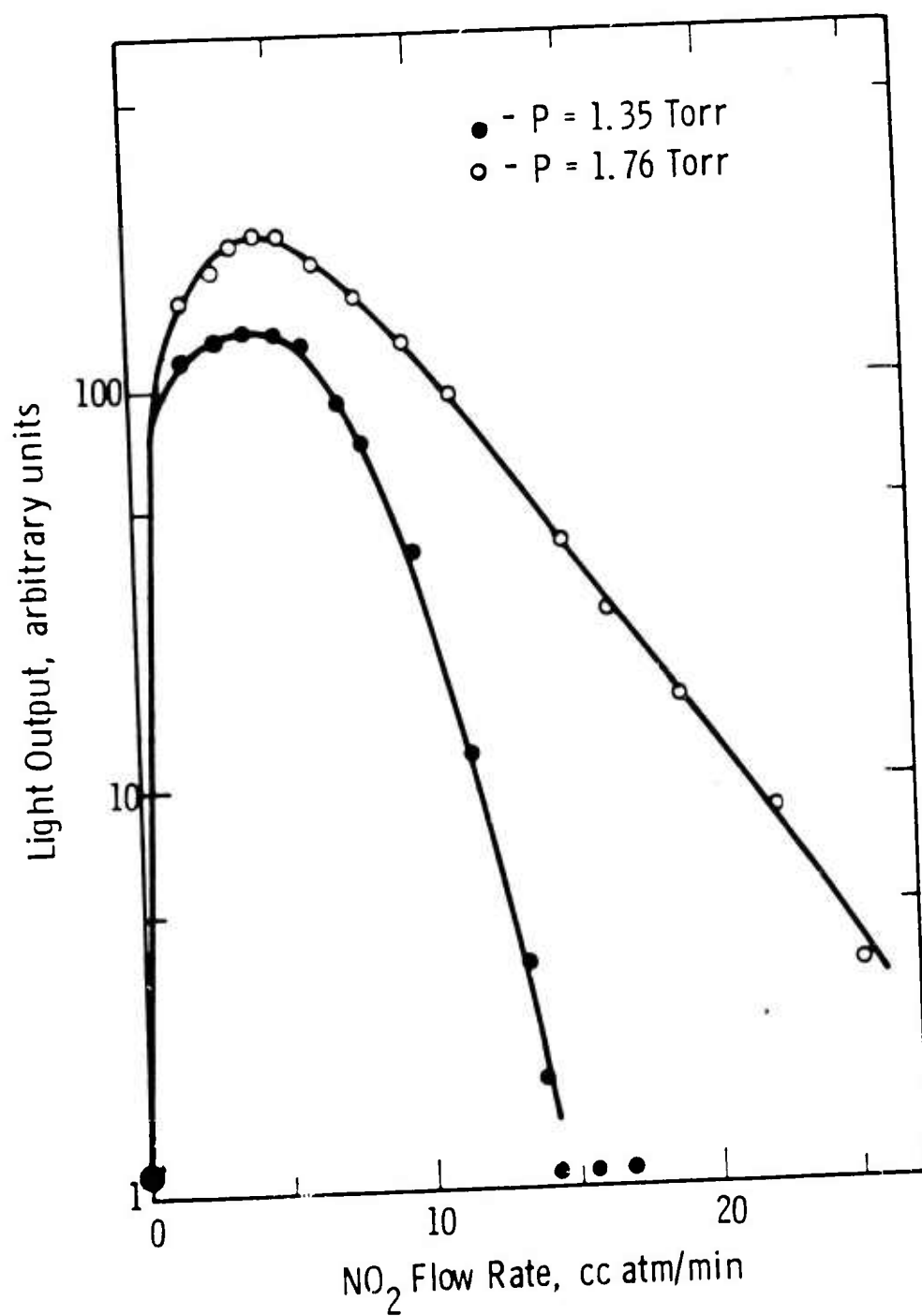
Fig. 9 Light output from the oxygen afterglow as a function of nitrogen dioxide flow rate.

the discharge and some NO_2 may possibly be diffusing into the discharge thus complicating the production and titration. Steps are now being taken to remedy this situation.

The decay of atomic oxygen along the tube can be determined by the addition of a small amount of NO_2 to the O_2-O mixture (just sufficient to produce an adequate afterglow along the tube) and observing the intensity decay as a function of distance with the photomultiplier. This decay can be attributed to the following reactions,

$$O + \text{wall} \rightarrow \frac{1}{2} O_2, \tag{9}$$

$$O + O_2 + M \rightarrow O_3 + M, \tag{10}$$

and

$$O + O_3 \rightarrow 2 O_2. \tag{11}$$

If any excited states of molecular oxygen are present, then atomic oxygen production can occur in regions other than the discharge region, since

$$O_3 + O_2^* \rightarrow O + 2 O_2 . \tag{12}$$

A typical atomic oxygen decay curve for the aluminum flow section is shown in Fig. 10.

(IV B.4) Production of O_2^-

In the electron gun region a swarm of electrons is emitted from a hot thoriated iridium filament, F, and crosses the gas stream under the influence of an electric field, E, applied between F and the collector C. By keeping the applied field sufficiently low ($E/p < 2$ $Vcm^{-1}Torr^{-1}$) no ionization can occur and attachment of electrons occurs only via the following reaction,[16]

$$O_2 + O_2 + e \rightarrow O_2^- + O_2. \tag{13}$$

If the applied field is reversed periodically at a frequency much greater than the reciprocal of the transit time of the ions, the
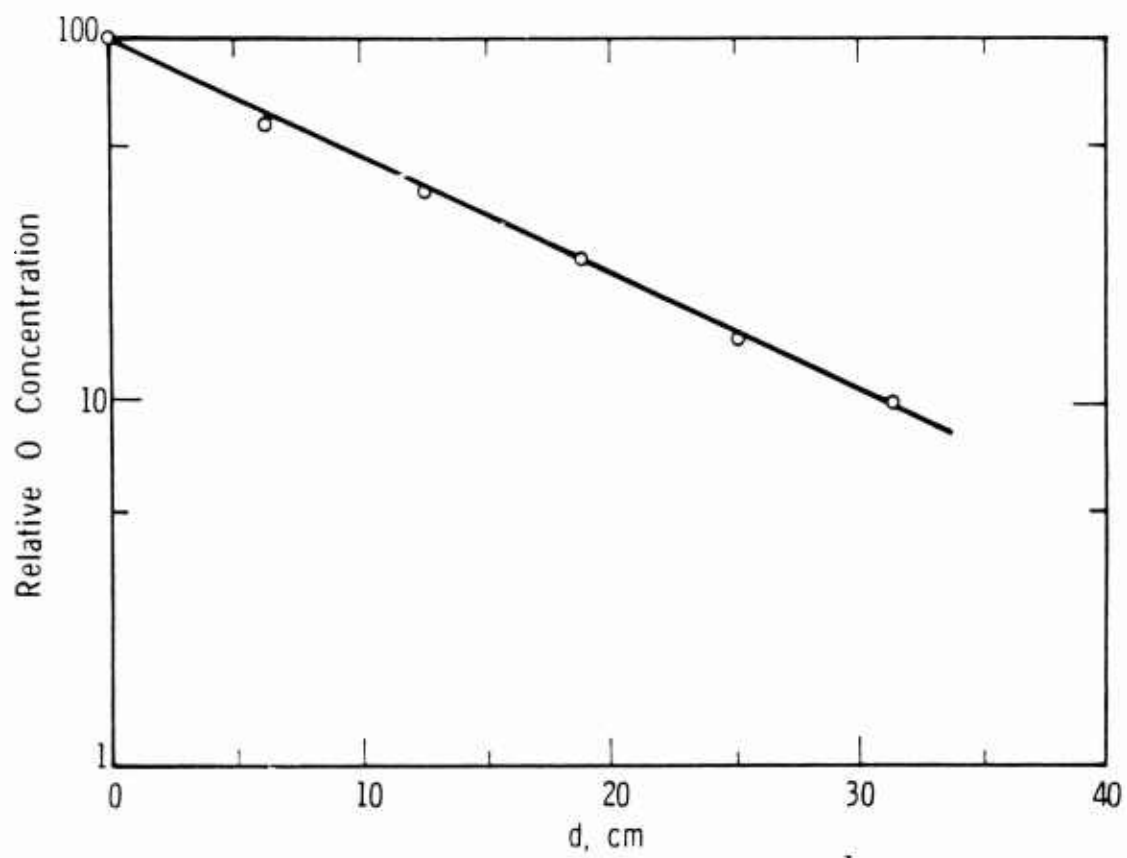
Fig. 10. Decay of atomic oxygen in the aluminum section of the flow tube.

resulting force on the ions due to the electric field is zero, and they will drift along the tube with the neutral gas mixtures.

By measuring the emitted electron current I_o, and the collected electron current I_e, the attachment coefficient η for the gas can be calculated, since

$$I_e = I_o \, e^{-\eta d} \tag{14}$$

where d is the spacing between the filament and collector. This gives reasonable agreement with previous determinations of η for undissociated oxygen.

Both negative ions and electrons have been detected in the detachment region. To collect electrons the rf voltage applied to any pair of grids is increased until the collected current saturates. Similarly to collect negative ions the applied dc voltage is increased until saturation occurs. Some typical data obtained in this manner are shown in Fig. 11.

(IV B.5) Measurement of Gas Velocities

The gas velocity v along the tube at pressure P_2 can be calculated from a knowledge of the gas input Q_1 at a pressure P_1. Since mass has to be conserved, the mass flow rates at both pressures are identical; thus, if the cross-sectional area of the tube is A, then

$$Q_1 P_1 = Q_2 P_2 = P_2 \, Av. \tag{15}$$

The viscous pressure drop per unit length along a tube of radius r can be calculated from the approximate Poiseuille equation

$$\Delta P = 1.18 \times 10^{-6} \, \frac{v}{r} \tag{16}$$

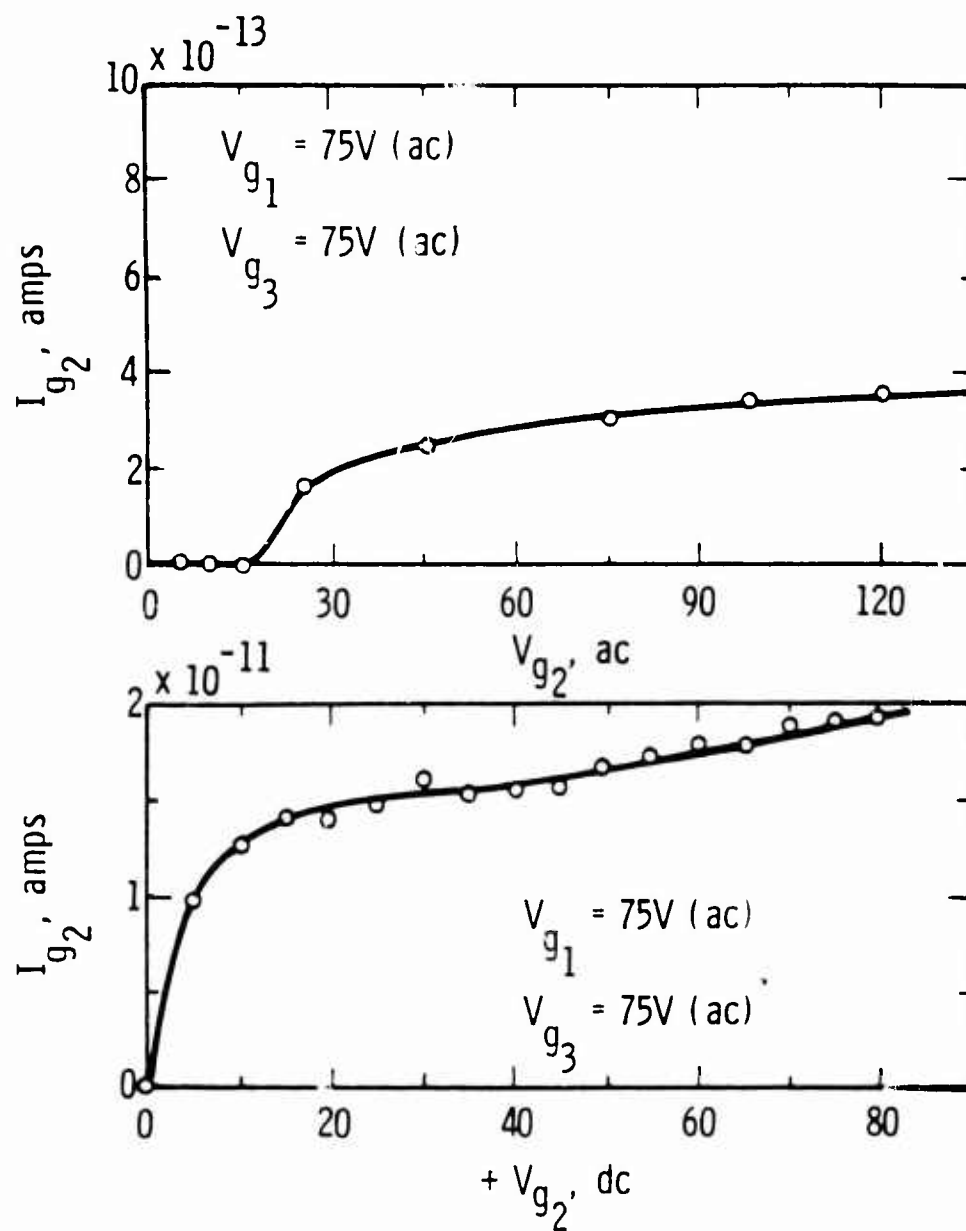and is found to be negligible at all times under our experimental conditions.

Fig. 11   Electron and negative ion currents in the detachment region.

31

Another method used to determine the gas velocity was to create a number of ions at a time t = 0 and allow them to drift a known distance before collection. This was done in the present system by pulsing the filament on for 1 msec and noting the time for the ions formed to drift to the first pair of rf grids. The agreement between the two methods at various pressures is $\approx 10\%$.

(IV B.6) Results of Flow Tube Experiments

The observed decay of atomic oxygen in the aluminum tube section is found to be exponential, see Fig. 10. If this decay is wholly attributed to wall collisions, a value for the surface recombination coefficient, γ, can be obtained. The value of γ calculated from the slope of Fig. 10 is 1.6×10^{-5} which is approximately the same value as the γ obtained by Kaufman[15] for pyrex glass. No information concerning the value of γ for aluminum could be found in the literature although most other common metals have been studied. This surprisingly low value of γ makes aluminum an extremely useful material for the construction of atomic oxygen flow systems if glass cannot be used. However, in this calculation of γ no account is taken of the loss of atomic oxygen due to collisional recombination by reactions such as given by Eq. (9), (10), and (11) or of its production from ozone and excited molecular oxygen, i.e., Eq. (12).

Enclosing the electron gun and detachment regions in an aluminum tube has reduced significantly the charging problems encountered in the all-glass flow tube and ion currents as low as 5×10^{-13}A can be detected in the detachment region. Thus, the use of aluminum provides us with a means of reducing charging currents to an acceptable level without increasing the rate of destruction of atomic oxygen.

Experiments performed before the system had been baked, i.e., a situation resulting in a fast decay of atomic oxygen along the tube, produces an electron current signal in the detachment region. The behavior of this current in response to changes in various experimental param rs is consistent with a detachment reaction between negative ions and some, as yet undetermined, neutral species produced in the discharge. However, after cleaning the walls of the flow tube by baking the system at 230°C, the atomic oxygen density increased at all points along the tube

32

and under these conditions all of the negative ions (presumably O_2^-) are destroyed before reaching the central electrodes in the detachment region. This situation prevails for all values of the discharge power input indicating that too much atomic oxygen (or excited molecular oxygen) is being produced by the discharge. Electron detachment now occurs while the negative ions are in a region controlled by the electron gun ac field thus enabling the detached electrons to be collected by the electrodes of the electron gun. Thus on initiating the discharge an increase of the electron current collected in the gun region of up to 30% was observed. However, it is difficult to assess the rate of the reaction under these circumstances since conditions in the gun are not as well defined as in the detachment region, but observations are consistent with a fast associative detachment reaction involving O_2^- and O, (or perhaps O_2^*). In the near future we shall attempt to decrease the concentration of the reacting neutral species by adding a buffer gas, perhaps argon, to the gas flowing through the discharge.

We also plan to modify the system to allow us to produce ground state atomic oxygen without also producing excited molecular oxygen. This technique for producing atomic oxygen involves dissociating nitrogen and then adding an equimolar amount of nitric oxide,[17]

$$N + NO \rightarrow N_2 + O \ .$$ (17)

By carrying the nitrogen through the discharge in a buffer gas, easy control of the final atomic oxygen density should be possible. A further advantage of this technique is that excited molecular nitrogen can be readily removed from the flow by the insertion of a glass wool plug into the stream.[13]

IV C. The Mass Spectrometer

(IV C.1) Description of the Mass Spectrometer and Test System

The mass spectrometer is housed in a stainless steel envelope and is connected to the ion source through a 0.01" dia. hole in an insulated, gold plated "nose." Neutral gas particles which succeed in entering the mass spectrometer chamber pass readily through the open structure of the mass spectrometer and are removed by the high speed pumping system. This pumping system consists of a one liter/sec rotary pump, a 720 liter/sec

33

diffusion pump and a 100 liter/sec liquid nitrogen trap, see Fig. 12.
Typically the pressure in the mass spectrometer is less than 10^{-3} Torr for
ion source pressures up to 10 Torr.

Any ions which enter the chamber are accelerated through a poten-
tial and enter the Boyd rf mass spectrometer,[9] which consists of 32 equally
spaced cylindrical elements, alternate elements being connected together.
A constant rf voltage is applied to these elements and an ion whose transit
time through one of the cylindrical elements equals an odd multiple of the
half period of the rf field will gain energy at each successive element and
is said to be "in resonance." These resonant ions gain sufficient energy to
overcome an adjustable discriminating potential and are then further
accelerated onto the first dynode of a nine stage secondary electron
multiplier, whose output is fed to an insulated vibrating reed electrometer.
The examination of negative ions requires that the detector be above ground
potential; thus, for small signals a "guarded" feedthrough to the electrom-
eter has been provided. The electrometer output is coupled (through a
servo mechanism) to a pen recorder which traces out the mass spectrum as the
frequency of the rf voltage is mechanically swept. Under typical operating
conditions, the resolving power of the instrument is ≈ 40.

The high pressure ion source used to test the mass spectrometer
consisted of a stainless steel chamber coupled to the front end of the mass
spectrometer chamber. A uniform field gap of 3 cms can be established
between the plate containing the 0.01" hole and a similar plate, see Fig. 12.
Two sources of electrons have been used. One technique consisted of placing
a hot filament on an equipotential line between the two electrodes. By
suitably arranging the potentials of the gap, electrons could be collected on
either electrode thus enabling either a positive or negative ion scan to be
made. However, in oxygen the filament lifetime is short. A suitably
constructed photo cathode was found to operate over long periods of time
without loss of emission. This photo cathode was fabricated by depositing
a thin gold layer (≈ 300 Å) on a quartz window supported on a suitable flange.
The gold film was the cathode, and contact to it was made through a stainless
steel spring, see Fig. 12. Placing a small uv lamp (≈ 10 watts; $\lambda \approx 2550$ Å)
directly behind the quartz window enabled electron emission currents of up
to 5×10^{-7} A to be obtained in vacuum. These currents drop to $\approx 10^{-8}$ A

34

R.F. Mass Spectrometer

Glass-Metal Seal

Multiplier

Output

Filament

Gas

Pump

UV Lamp

300Å Gold

Quartz Window
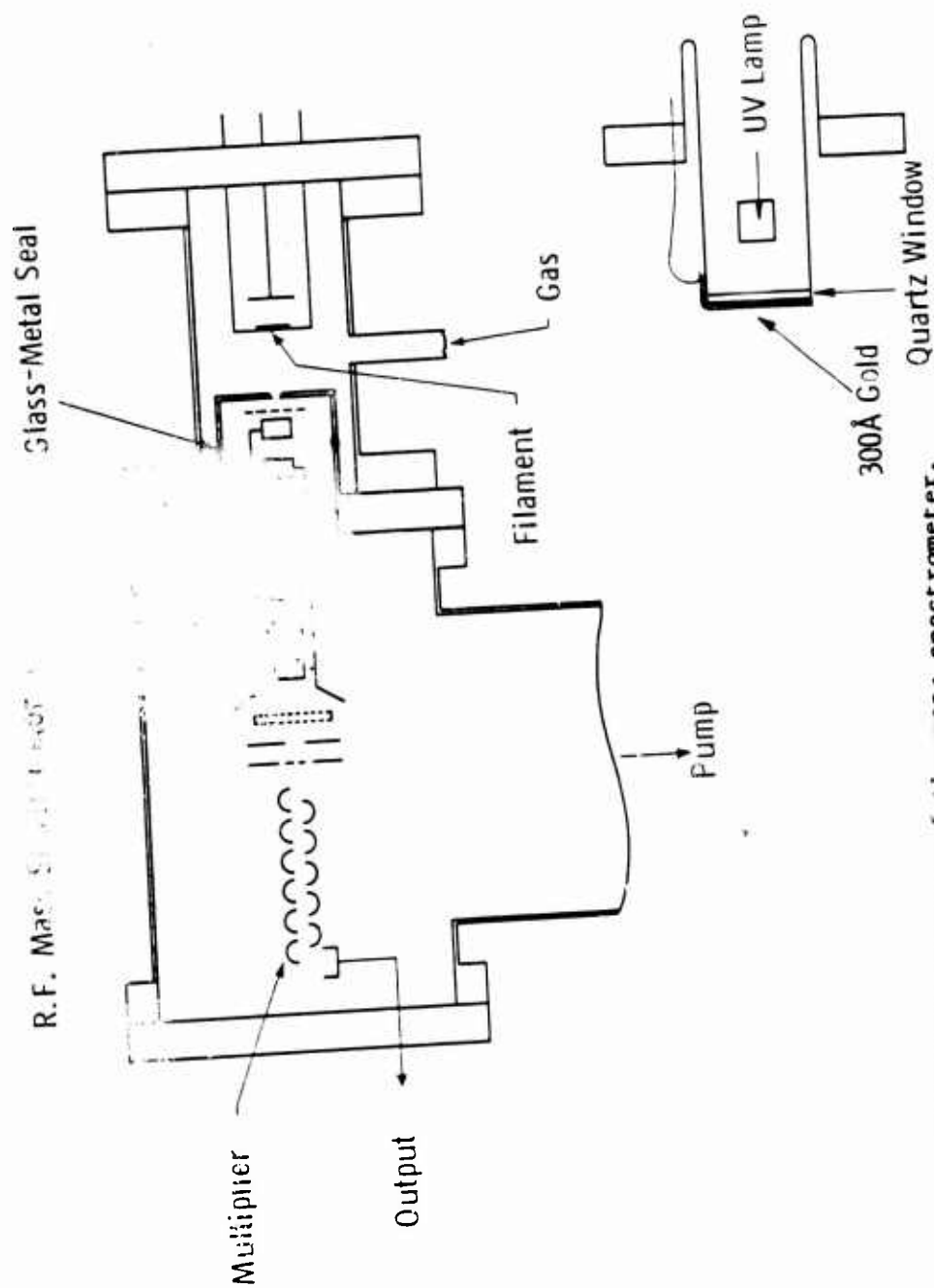
12 Schematic diagram of the mass spectrometer.

35

when gas is admitted to the cell but are still sufficiently large to operate the mass spectrometer. Although only negative ions can be examined using this source, it has proved to be most useful since it can perform for many months in various gases without degradation.

Initial testing of the mass spectrometer was performed using oxygen as the test gas but, as the instrument was improved, the negative ion spectra of CO_2, H_2O, and CO_2-O_2 and N_2-O_2 mixtures were also examined. Two variable leak inlet valves were used to produce the required gas mixtures, and the input to the gas cell was adjusted to compensate for the gas lost through the 0.01" hole to the mass spectrometer pumps.

After the spectrometer was properly tuned, the negative ion mass spectrum of O_2, N_2, $_2$ and H_2O as well as mixtures of CO_2-O_2, N_2-O_2, and H_2O-O_2 were examined as a function of both E/p and pressure. Source pressures between '   and 5 Torr were used, the lower pressures being measured on a calibrated high pressure ionization gauge while pressures above $\approx$ 1 Torr were measured on a differential oil manometer. Both the uv photocathode and hot filament were used as electron sources in these experiments and yielded similar results, the only difference being that the filament tended to cause a small increase in the apparent E/p which can be attributed to the filament voltage drop distorting the local electric fields. All the data to be presented in this report were taken using the uv electron source. A typical mass scan for an H_2O-O_2 gas mixture is shown in Fig. 13. No attempt has been made to correct   ion peak heights for the sensitivity of the ion multiplier to the mass of the impinging ions or to correct for the change in D/μ of the ions in the source as the source pressure is altered. However, with the uv photocathode it is felt that this latter effect is small since electrons are emitted from a large surface area.

When the mass spectrometer is finally coupled to the flow system, the ion signals in the detachment region will probably be very weak. Therefore, the possibility of adapting the detection system to the use of counting techniques is being investigated.
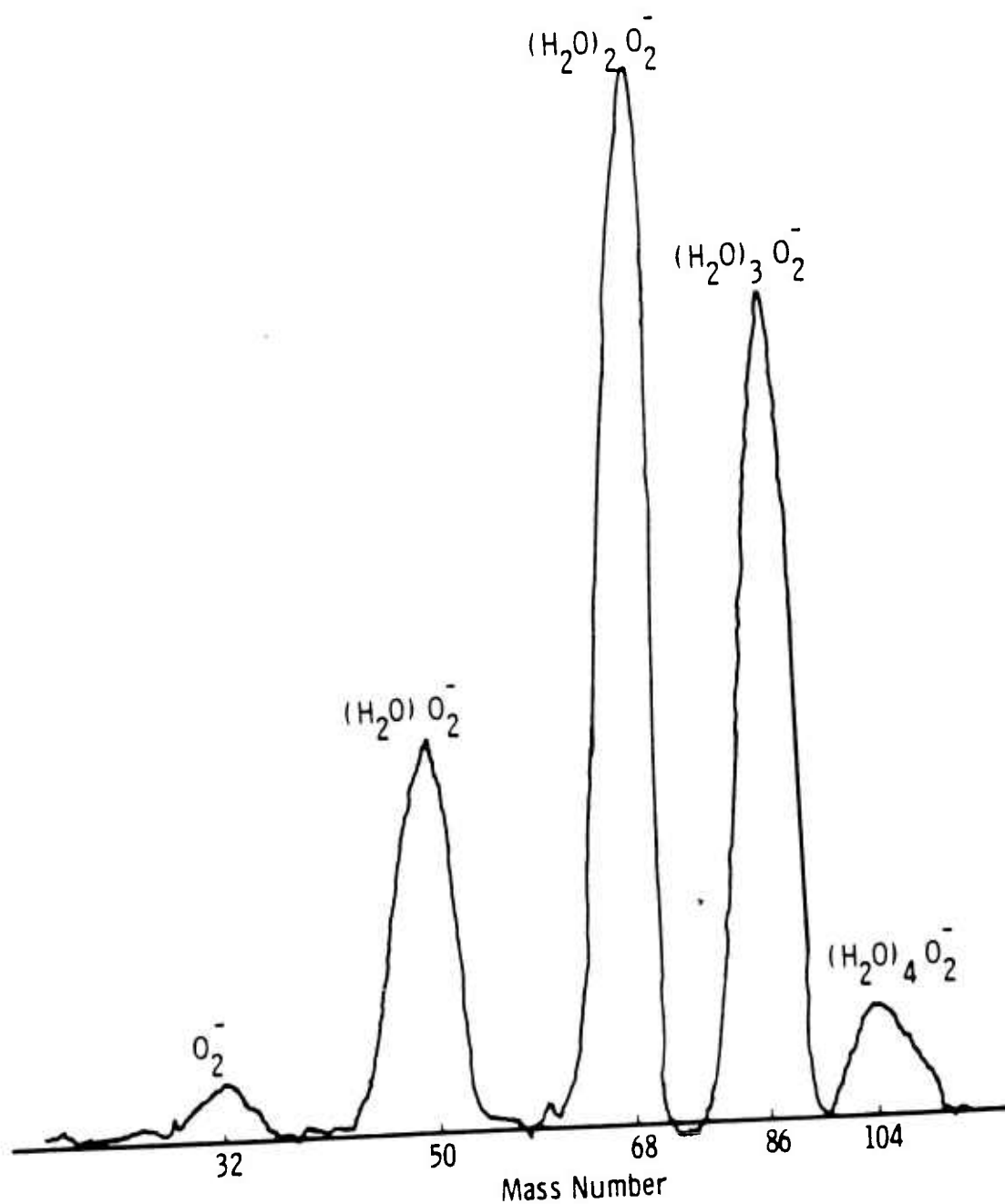
Fig. 13 The mass spectrum of an H_2O-O_2 mixture at an E/p of 0.83 V cm^{-1}Torr^{-1}.

(IV C.2)   Results of Mass Spectrometer Experiments

In the process of testing the mass spectrometer useful information
concerning the negative ion species produced in various gases and gas
mixtures has been obtained. In particular, it has been established that in
oxygen three negative ions can be produced, see Fig. 14. At low values of
E/p, below ≈ 2 Vcm^{-1} Torr^{-1}, O_2^- is the only ion formed, confirming the
conclusions of Chanin, Phelps and Biondi.[16] This ion is formed by the three-
body attachment reaction given by Eq. (13).

At higher values of E/p, O^- formed by a dissociative attachment
reaction is the primary negative ion produced, i.e.,

$$O_2 + e \rightarrow O^- + O_2. \tag{18}$$

This reaction is followed by one of two ion-molecule reactions producing
either O_3^- or O_2^-, i.e., by

$$O^- + O_2 + O_2 \rightarrow O_3^- + O_2 \tag{19}$$

or $$O^- + O_2 \quad \rightarrow O_2^- + O. \tag{20}$$
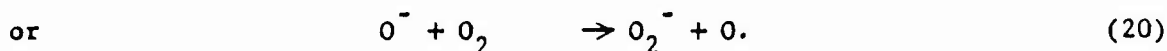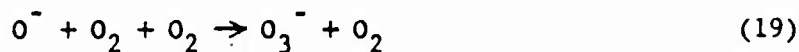
By arranging the source conditions such that only two ions are present, the
rates of the ion-molecule reactions can be determined, since

$$\frac{I_{O_3^-}}{I_{O^-}} = \frac{\alpha(1-e^{-\beta N^2 L}) - \beta N (1-e^{-\alpha NL})}{\alpha(e^{-\beta N^2 L} - e^{-\alpha NL})} \tag{21}$$

where α and β are the rates of Eqs. (18) and (19), respectively, N is the
neutral gas density and L is the electron path length. Thus, by plotting
the ratios of O_3^-/O^- and O_2^-/O^- currents as functions of pressure, see Fig.
15, the rates of the reactions given by Eqs. (19) and (20) were found to be
1.5×10^{-31} cm^6 sec^{-1} and 3.74×10^{-13} cm^3 sec^{-1}, respectively. The rate for
Eq. (19) has been given by Beaty, et al.[18] as 9.1×10^{-30} cm^6 sec^{-1}.
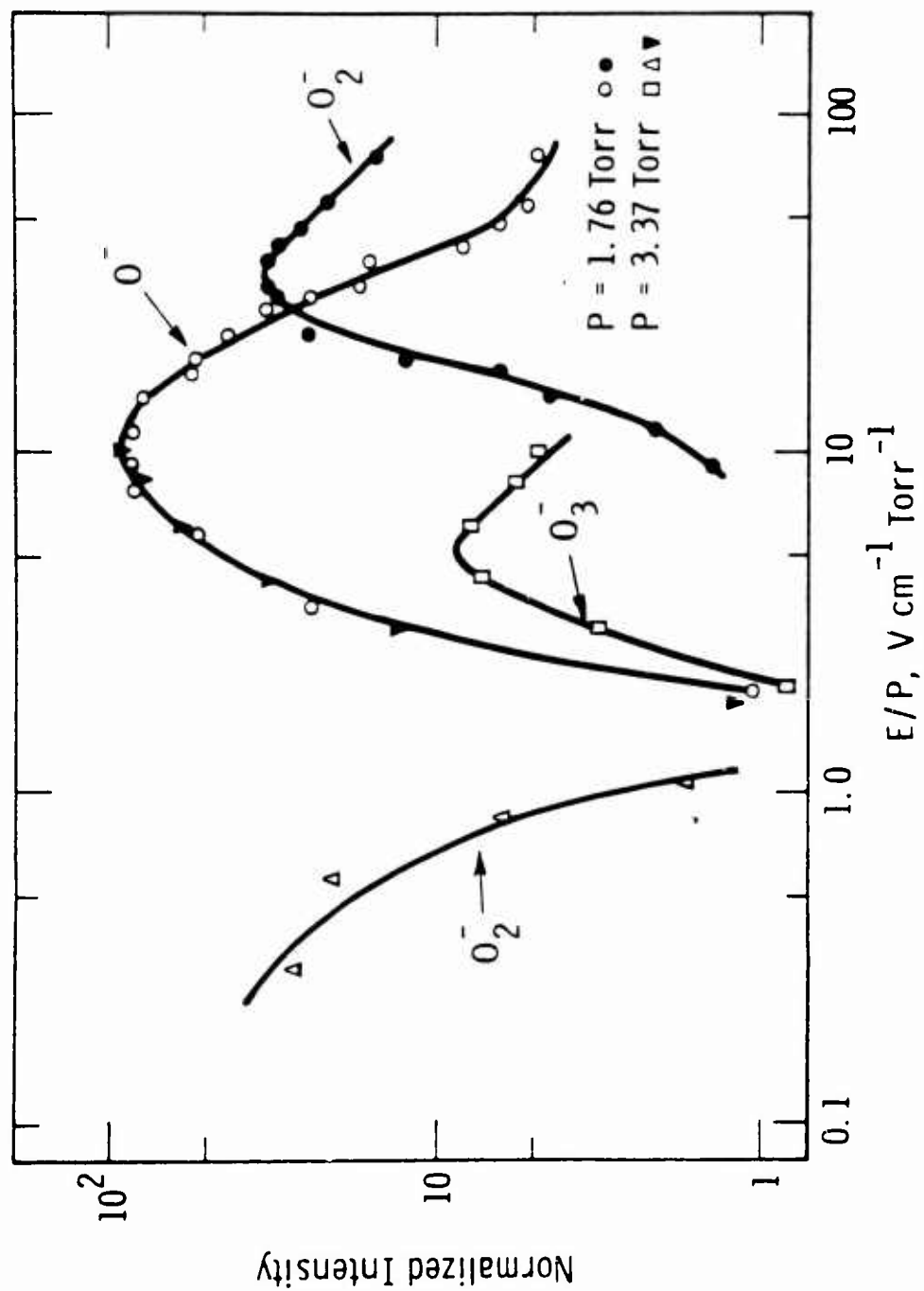
38

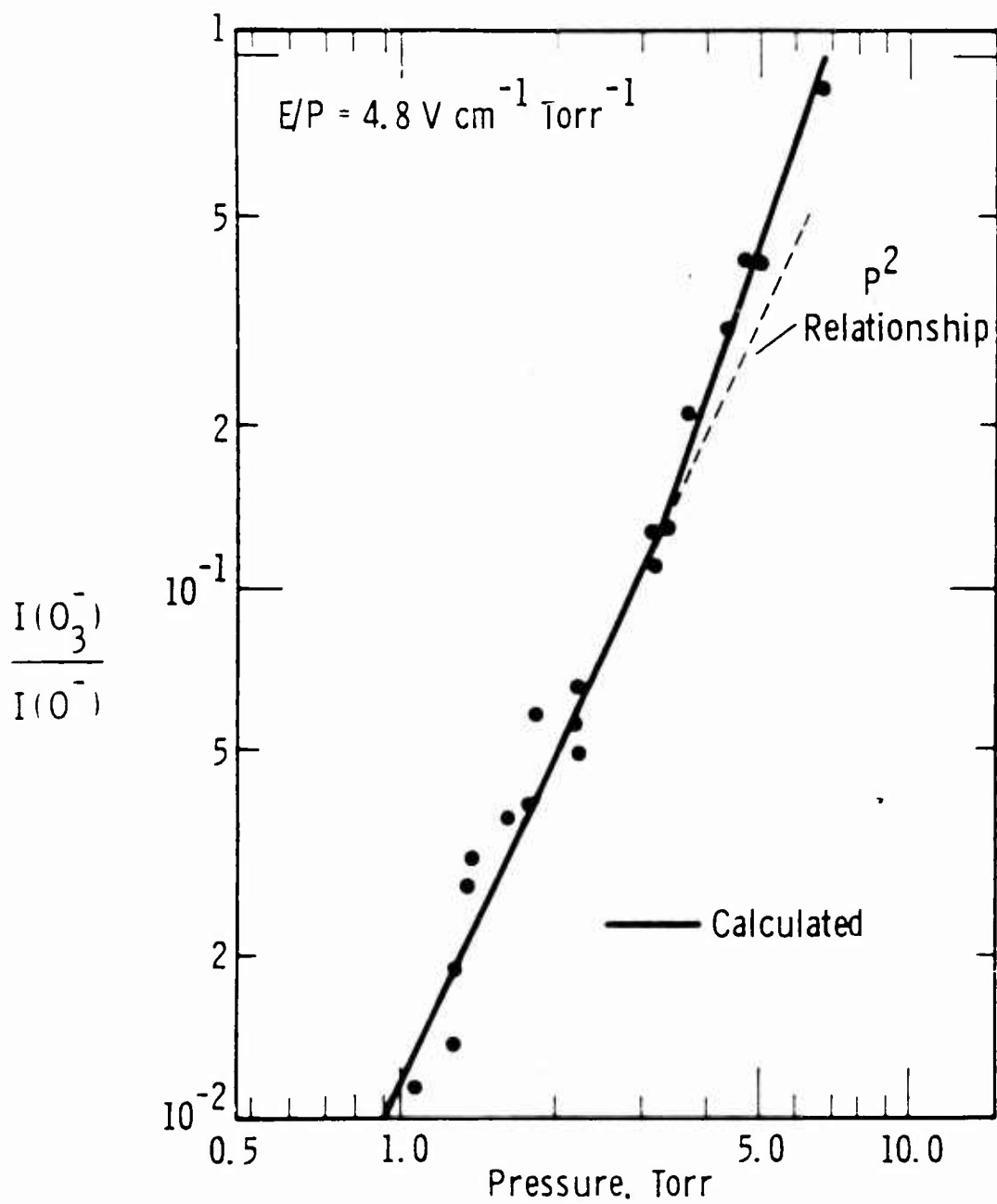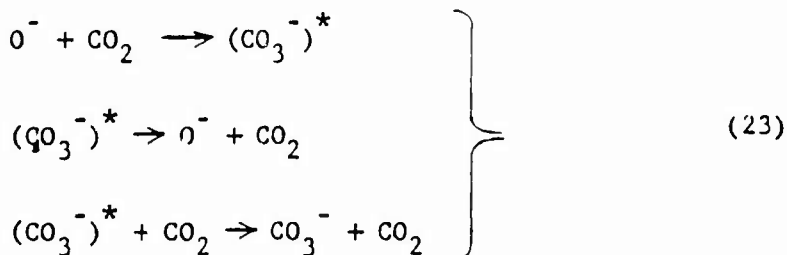Fig. 14 Ion intensity as a function of E/p in oxygen.

Fig. 15 Pressure dependence of $I(O_3^-)/I(O^-)$ in oxygen.

40

In pure CO_2 no negative ions were observed at low values of E/p but for values greater than ≈ 7 Vcm^{-1}Torr^{-1}, two ions 0^- and CO_3^- were detected. It was established that the reactions involved were

$$CO_2 + e \rightarrow CO + O^- \tag{22}$$

$$\left.\begin{array}{l} O^- + CO_2 \longrightarrow (CO_3^-)^* \\[1em] (CO_3^-)^* \rightarrow O^- + CO_2 \\[1em] (CO_3^-)^* + CO_2 \rightarrow CO_3^- + CO_2 \end{array}\right\} \tag{23}$$

Using a similar technique, see Fig. 16, to that described above the rate for Eq. (23) was found to be 1.3×10^{-28} cm^{6}sec^{-1}.

When oxygen is added to CO_2, four negative ions were observed, see Fig. 17. At low energies O_2^- produced by three-body attachment is the primary ion formed (in O_2 - CO_2 mixtures the third body for this reaction can be either O_2 or CO_2). This O_2^- then undergoes the following reaction,

$$O_2^- + CO_2 + X \rightarrow CO_4^- + X \tag{24}$$
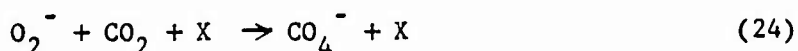
with an approximate rate of 1.28×10^{-29} cm^{6}sec^{-1}. The formation of a complex negative ion under these conditions has been observed by Phelps and Pack[19] who, on the basis of the law of mass action, predicted its identity as being CO_4^-. At higher values of E/p the reactions of Eq. (22) and (23) are again observed.

In pure water seven negative ions were observed for E/p > 10 V cm^{-1}Torr^{-1}, see Fig. 18, but none were detected at lower electron energies. Clustering of positive ions in water has been observed,[20,21] but there are no such reports involving negative ions. One possible mechanism for the formation of these ions is the following. Initially dissociative attachment producing H^- occurs[22]

$$H_2O + e \rightarrow H^- + OH \tag{25}$$

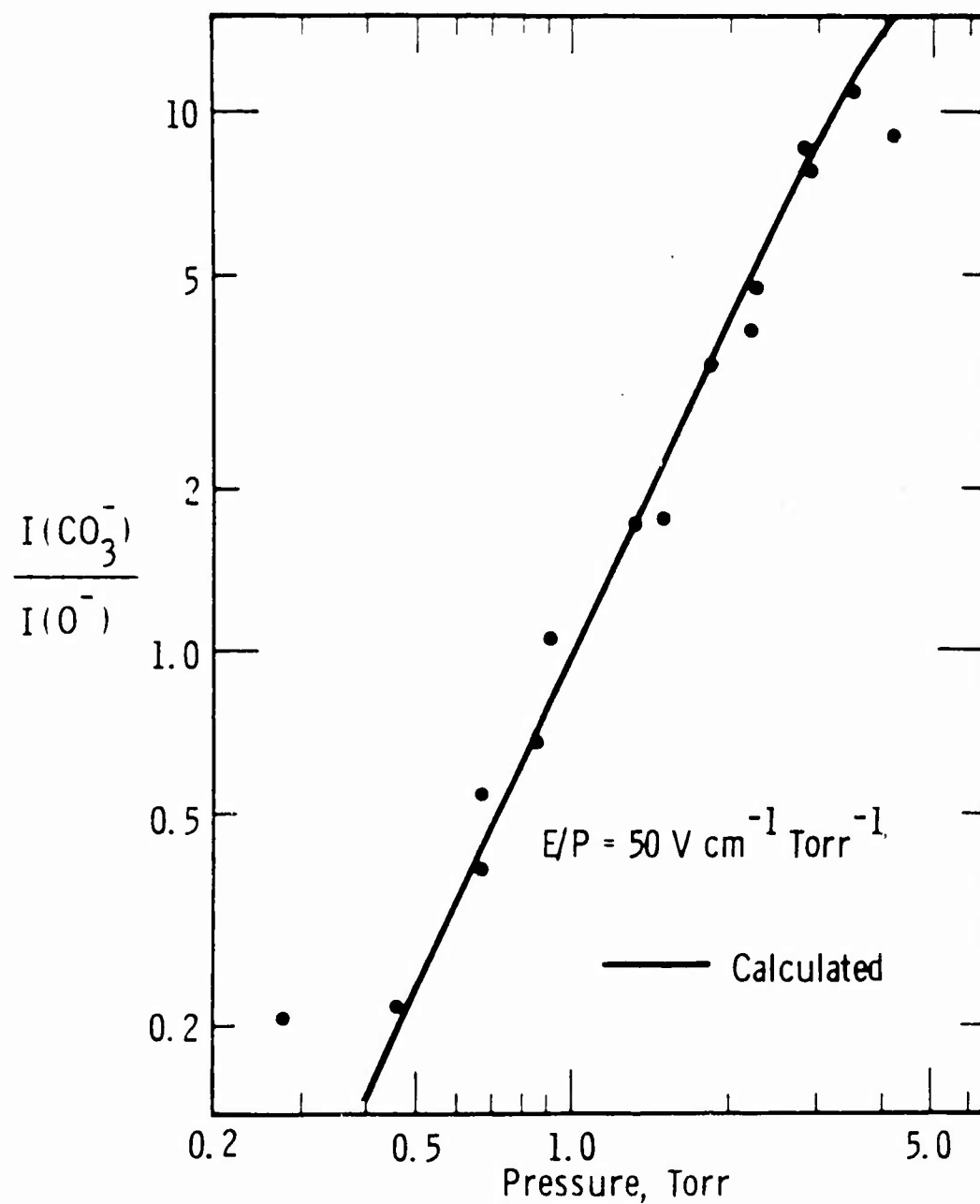Fig. 16 Pressure dependence of $I(CO_3^-)/I(O^-)$ in carbon
dioxide.
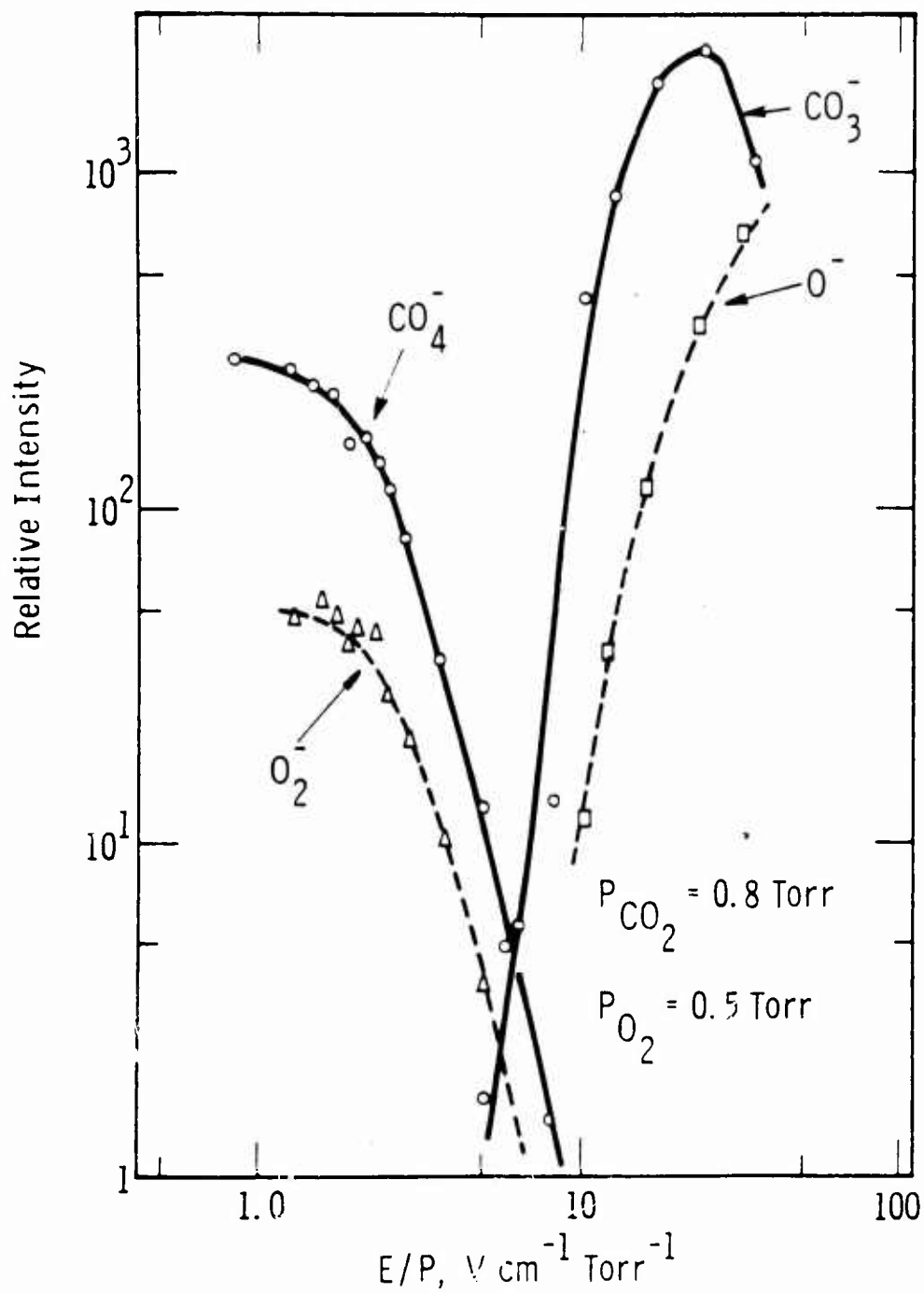
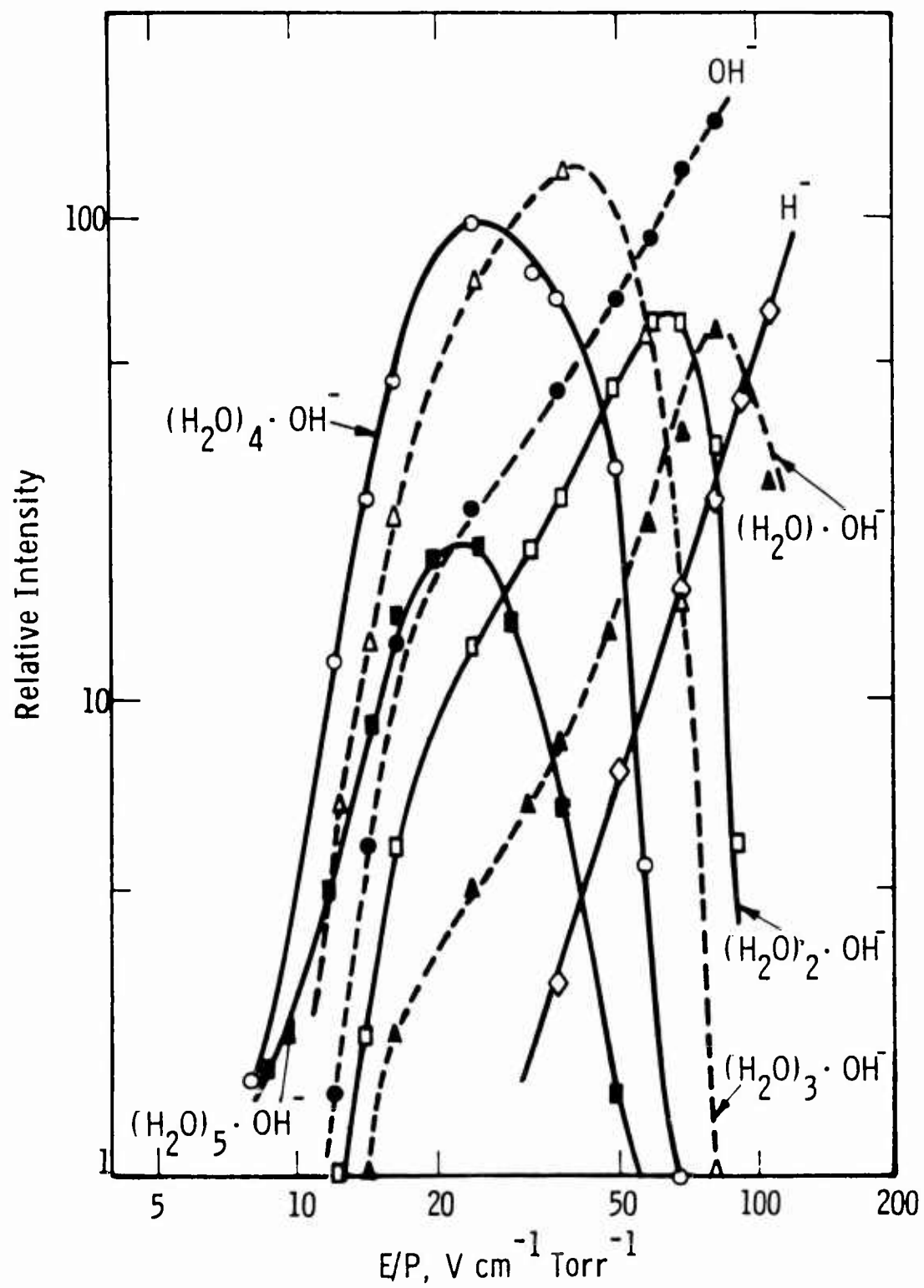Fig. 17 Ion intensity as a function of E/p in a CO_2-O_2 mixture.

43

Fig. 18 Ion intensity as a function of E/p in water vapor.

44

which is then followed by,[23]

$$H^- + H_2O \rightarrow OH^- + H_2 \tag{26}$$

since this is exothermic by at least 0.3 eV. Clustering of OH^- with various numbers of H_2O molecules then occurs probably by three-body reactions,

$$OH^- + H_2O + H_2O \rightarrow (H_2O) \cdot OH^- + H_2O. \tag{27}$$
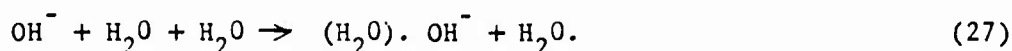
The heavier negative ions, e.g., $(H_2O)_5 \cdot OH^-$, are the least stable as can be seen from Fig. 18 where the dominant ion becomes less and less complex as the ion energy is increased by increasing E/p. Finally, only H, OH^- and $(H_2O) \cdot OH^-$ are observed at an E/p of 100 $Vcm^{-1} Torr^{-1}$. If oxygen is now added to the system the situation becomes even more complex. At low values of E/p, O_2^- is again initially formed by the three-body attachment reaction and this ion then proceeds to form clusters with various numbers of water molecules, see Fig. 19. The probable reactions leading to the formation of these ion clusters are,

$$O_2^- + H_2O + X \rightarrow (H_2O) \cdot O_2^- + X \tag{28}$$

$$(H_2O) \cdot O_2^- + H_2O + X \rightarrow (H_2O)_2 O_2^- + X \tag{29}$$

$$(H_2O)_{n-1} \cdot O_2^- + H_2O + X \rightarrow (H_2O)_n \cdot O_2^- + X \tag{30}$$
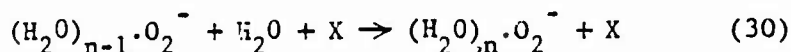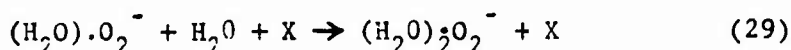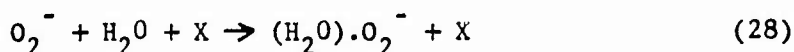
Complex negative ions with n = 1,2,3,4 and 5 have been observed. Attempts to reduce the complexity of the situation by reducing the partial pressure of H_2O in the mixture were only partially successful. If the partial pressure of H_2O is less than 10^{-4} Torr only three negative ions are produced, i.e., O_2^-, $(H_2O) \cdot O_2^-$ and $(H_2O)_2 \cdot O_2^-$. Conditions in which O_2^- and one complex ion were present were never attained; thus, the determination of the rate of these reactions was not attempted. Although no quantitative information was obtained from this experiment, it indicated that the formation of $(H_2O)_2 \cdot O_2^-$ proceeds at an extremely fast rate ($> 10^{-28} cm^6 sec^{-1}$) and clearly demonstrates the precautions which have to be taken in
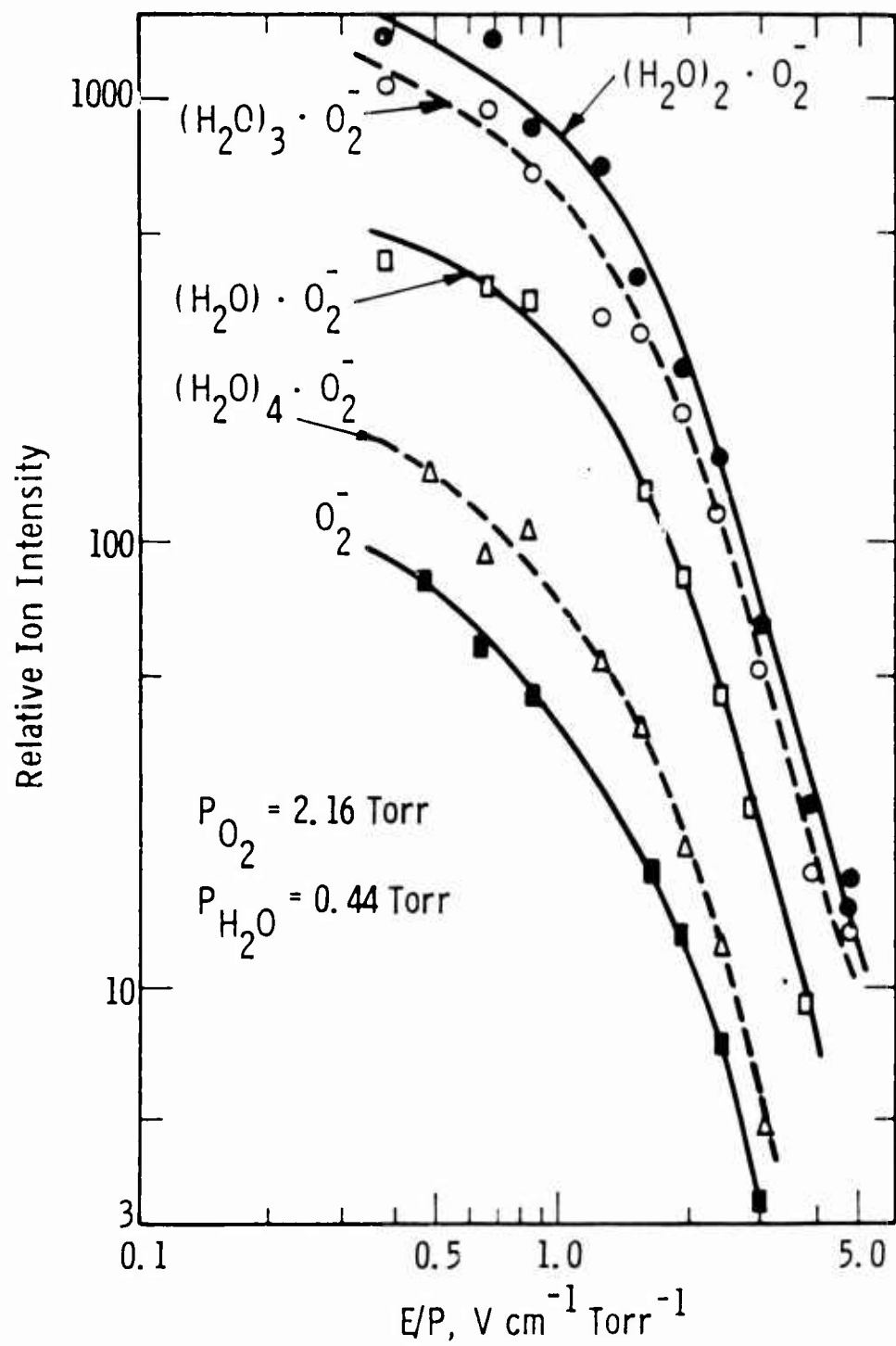
Fig. 19 Ion intensity as a function of E/p in a H_2O-O_2 mixture.

The figure plots Relative Ion Intensity (vertical axis, logarithmic from 3 to 1000) against E/P, $V\ cm^{-1}\ Torr^{-1}$ (horizontal axis, logarithmic from 0.1 to 5.0). Curves are labeled $(H_2O)_3 \cdot O_2^-$, $(H_2O)_2 \cdot O_2^-$, $(H_2O) \cdot O_2^-$, $(H_2O)_4 \cdot O_2^-$, and O_2^-. Conditions: $P_{O_2} = 2.16$ Torr, $P_{H_2O} = 0.44$ Torr.

experiments involving low energy negative ions. It also suggests that hydrated negative ions are to be expected in the earth's atmosphere wherever there is significant H_2O concentration.

At higher values of E/p, > 6 $Vcm^{-1}Torr^{-1}$, O^- is initially formed, followed by many clustering reactions, similar to those described above to produce $(H_2O)_n \cdot O^-$. Ionr with n = 1,2,3,4 and 5 were detected.

The negative ion spectrum of molecular nitrogen was also studied, but no negative ions were detected. Mixtures of nitrogen and oxygen formed no complex ions. At low values of E/p, O_2^- was present while at higher values O^- and O_3^- were detected as expected.

MOMENTUM TRANSFER AND INELASTIC CROSS SECTIONS FOR ELECTRONS IN O_2

V A. Introduction

This section presents the results of our attempts to calculate the momentum transfer and inelastic cross sections for electrons in O_2 from available experimentally measured values of transport coefficients for electrons under the influence of dc electric fields. Our results are most accurate for the determination of the cross sections for momentum transfer and vibrational excitation. Significant information has been obtained concerning the excitation of the lower lying electronic states in O_2. Some information about rotational excitation and the excitation of the higher electronic states in O_2 has also been obtained. Unfortunately, the momentum transfer cross section obtained from the dc data disagrees with that obtained from analyses of microwave measurements. Further work is necessary to resolve this discrepancy.

The present results represent an extension of previous determinations of cross sections in H_2[24,25] D_2,[25] N_2[24,26] and the rare gases.[27] The technique is virtually unchanged from that described in Frost and Phelps[24] and Engelhardt and Phelps,[25] so a detailed discussion will be omitted. Briefly we solve numerically the time and space independent Boltzman transport equation for the distribution function of electron energies in a neutral gas, using an initial set of elastic and inelastic cross sections. Transport coefficients are calculated by taking suitable averages[24,25] over this distribution function, and are compared with experimental values of the same transport coefficients. The initial cross sections are then successively modified and the procedure repeated in order to obtain better agreement with the experimental transport coefficients. The cross sections are considered satisfactory when our calculated values match the experimental values to within 5% over an extended range of field strengths.

Two methods of solving the Boltzmann equation are discussed in the appendix of Reference 24, a) an "exact" solution for field strengths which are low enough such that the electrons are near thermal equilibrium, and it is necessary to consider collisions of the second kind, i.e., super-elastic collisions, and b) a solution neglecting collisions of the second

kind. In most of our present calculations we have employed the latter solution. However, when considering ϵ_k values close to kT, it is necessary to include collisions of the second kind. Here ϵ_k is the characteristic energy of the electrons, k is the Boltzmann constant and T is the gas temperature. In the case of O_2 an exact solution of the Boltzmann equation would include approximately as many rotational levels as previously[24-26] required for N_2 and would be valid only over a very limited range of ϵ_k/kT for $T \leqslant 77^\circ K$. We have developed an approximate solution for low values of ϵ_k/kT in which the effect of the many rotational energy levels is approximated by a single rotational level with a threshold at 5 kT/2 and a magnitude which gives results consistent with the continuous approximation of Reference 24 at large values of ϵ_k/kT. This approximation is used in our calculations for O_2 at low ϵ_k/kT.

As in previous analyses[24-27] we have facilitated the cross section determinations by employing two combinations of measured transport coefficients: a) the momentum transfer collision frequency ν_m, defined by

$$\nu_m/N = (e/m)E/Nw , \qquad (31)$$

which is primarily sensitive to the cross section for momentum transfer, and b) the energy exchange collision frequency ν_u, defined by

$$\nu_u/N = \frac{ew(E/N)}{\epsilon_k - kT} \qquad (32)$$

which is primarily sensitive to the inelastic cross sections. Here e and m are the charge and the mass of the electron, w is the electron drift velocity, E is the applied electric field and N is the gas density. We note that the characteristic energy ϵ_k is equal to eD/μ where D and μ are the electron diffusion and mobility coefficients, respectively.

The determination of elastic and inelastic scattering cross sections for electrons in oxygen is of particular interest because of the importance of oxygen in the ionosphere. The experimental[28-39] values of the dc transport coefficients w and ϵ_k are shown as points in Fig. 20. As suggested by the limited range of the ϵ_k values and the large scatter in
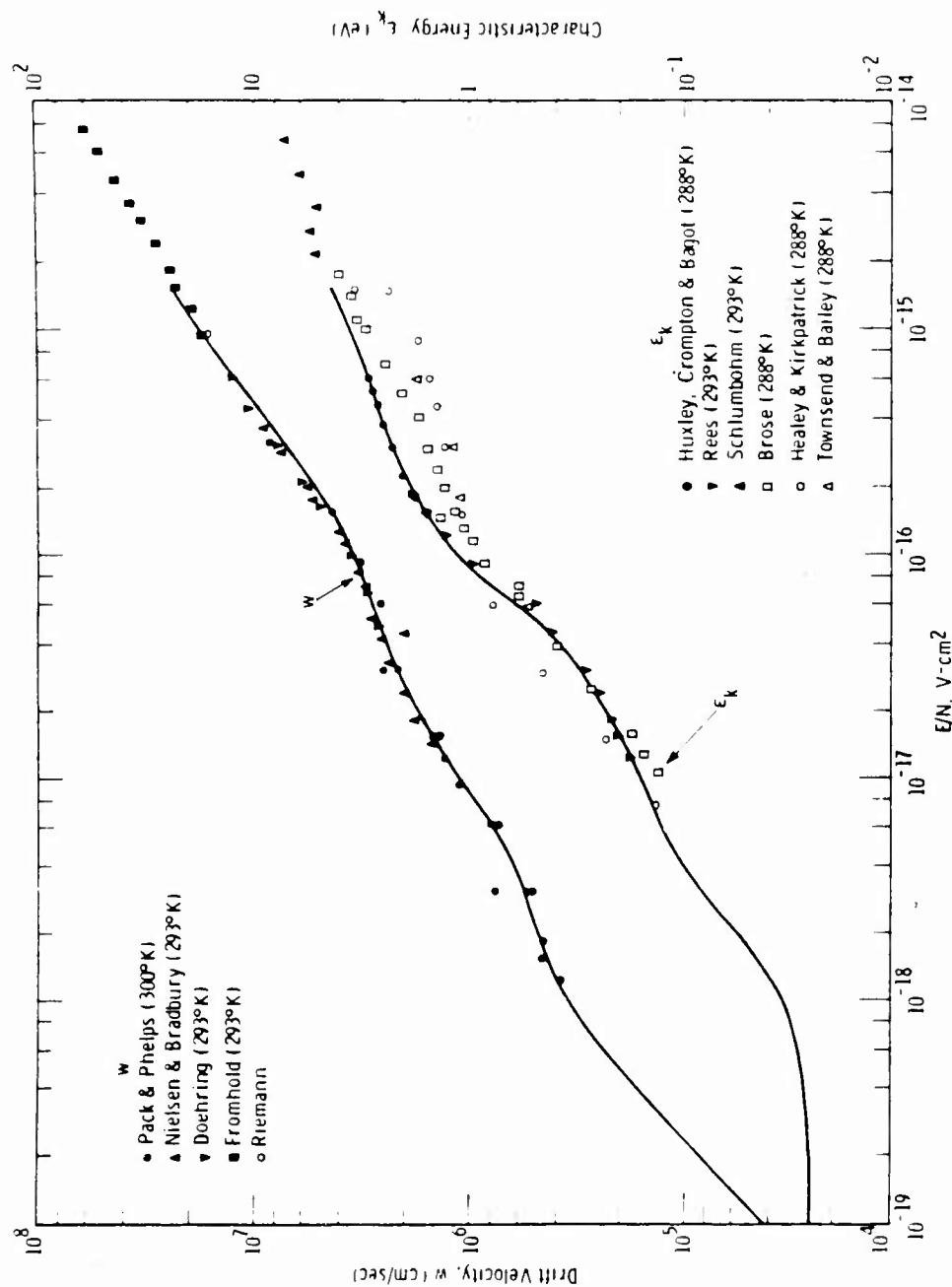
49

Fig. 20 Experimental and theoretical drift velocities and characteristic energies for electrons in oxygen. A smooth curve through the w and ϵ_k data shown by the solid points was used to construct the ν_m/N and ν_u/N curves of Fig. 21.

50

the data, the measurements of transport coefficients in O_2 are considerably more difficult than in non-attaching gases such as N_2 and H_2. We have based our analysis on the more recent results[35,37,38] for ϵ_k and have used these to construct the solid curves of ν_m/N and ν_u/N of Fig. 21. We also make use of the measured electron attachment coefficients,[16,39-42] α_a/N, and first Townsend ionization coefficients, α_1/N, shown by points in Fig. 22. The cross sections required to fit the measured transport coefficients are shown in Figs. 23 and 24. The smooth curves of Fig. 20 and the points of Fig. 21 show the transport coefficients calculated using these cross sections. As suggested by the structure in the ν_u/N curve of Fig. 21, it is convenient to divide our discussion into a low energy region, $\epsilon_k < 1.0$ eV, and a moderate energy region, 1.0 eV $< \epsilon_k < 3.0$ eV.

V B. Low Energies ($\epsilon_k < 1.0$ eV, $E/N < 10^{-16}$V cm^2)

In the low energy region the important inelastic collision processes in O_2 are rotational excitation, vibrational excitation and, possibly, electronic excitation of the $a^1\Delta_g$ and $b^1\Sigma_g^+$ levels with thresholds at 0.98 and 1.63 eV, respectively. This is also the range of energies for which electron attachment occurs predominantly by the three-body process.[16,43] Since ϵ_k measurements are not available below 0.15 eV and since the threshold for vibrational excitation is 0.195 eV, we will obtain very little information about rotational excitation. Since electron beam studies in this energy range[44] yield only the integrated values of the excitation cross sections near thresholds and since there are no theoretical cross sections for vibrational or electronic excitation, we are faced with an infinity of possible choices.

It appears that the assumption which is most consistent with all of the available experimental data is that the vibrational excitation cross sections consist of a set of narrow spikes delayed in energy relative to the vibrational excitation thresholds.[44,45] This assumption is easily made consistent with the small values of the integrated cross sections near threshold measured by Schulz and Dowell[44] and with the large cross sections required to explain the values of ν_u/N shown in Fig. 21. If the set of resonant type cross sections is assumed to be connected with the formation

51
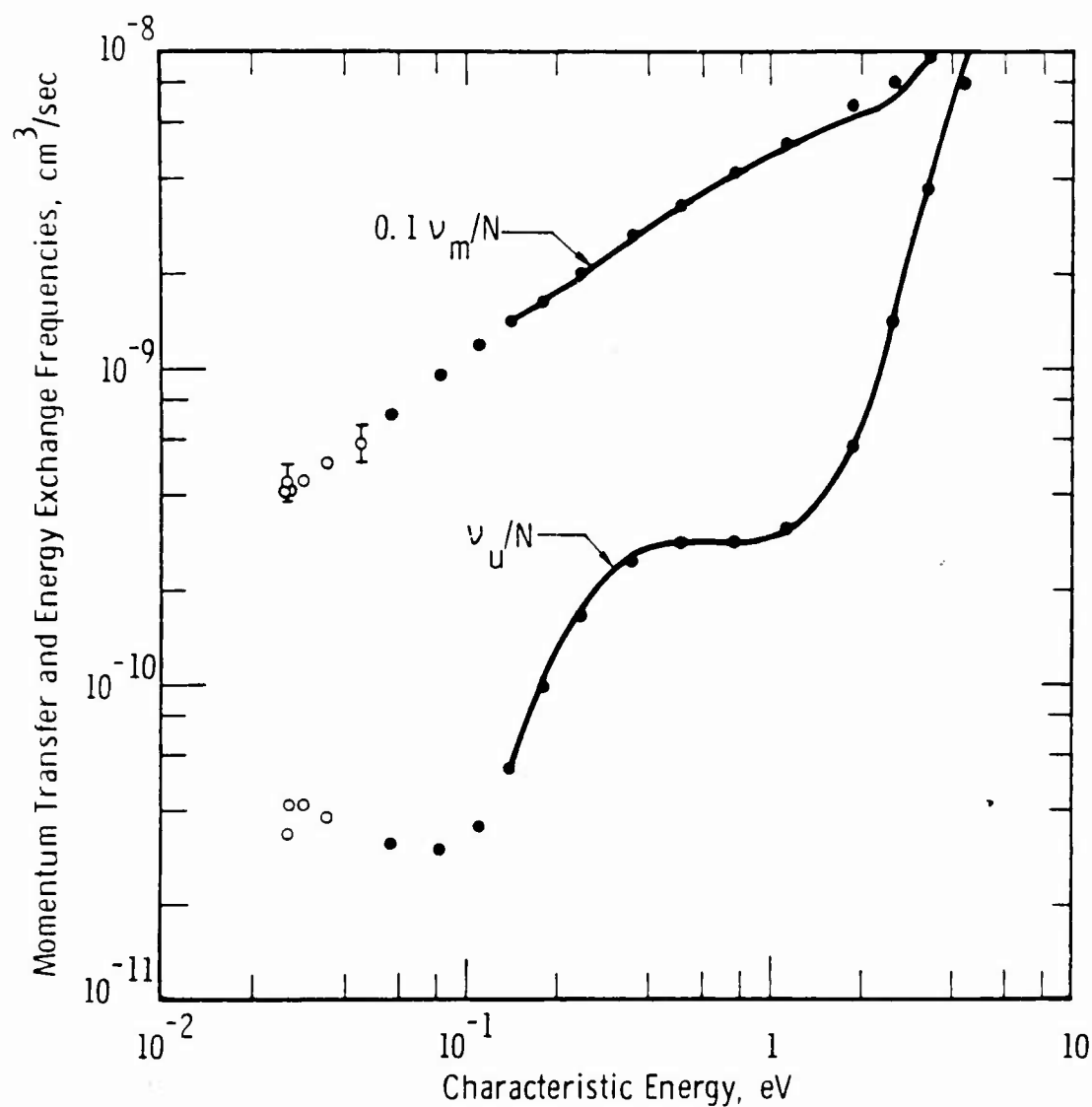
Fig. 21 Momentum transfer and energy exchange collision frequencies for electrons in oxygen. The solid curves are calculated from the experimental data of Fig. 20. The solid circles were calculated using the excitation cross sections discussed in the text and the continuous approximation to rotational excitation. The open circles were calculated using the single level approximation to rotational excitation as discussed in the text.

52
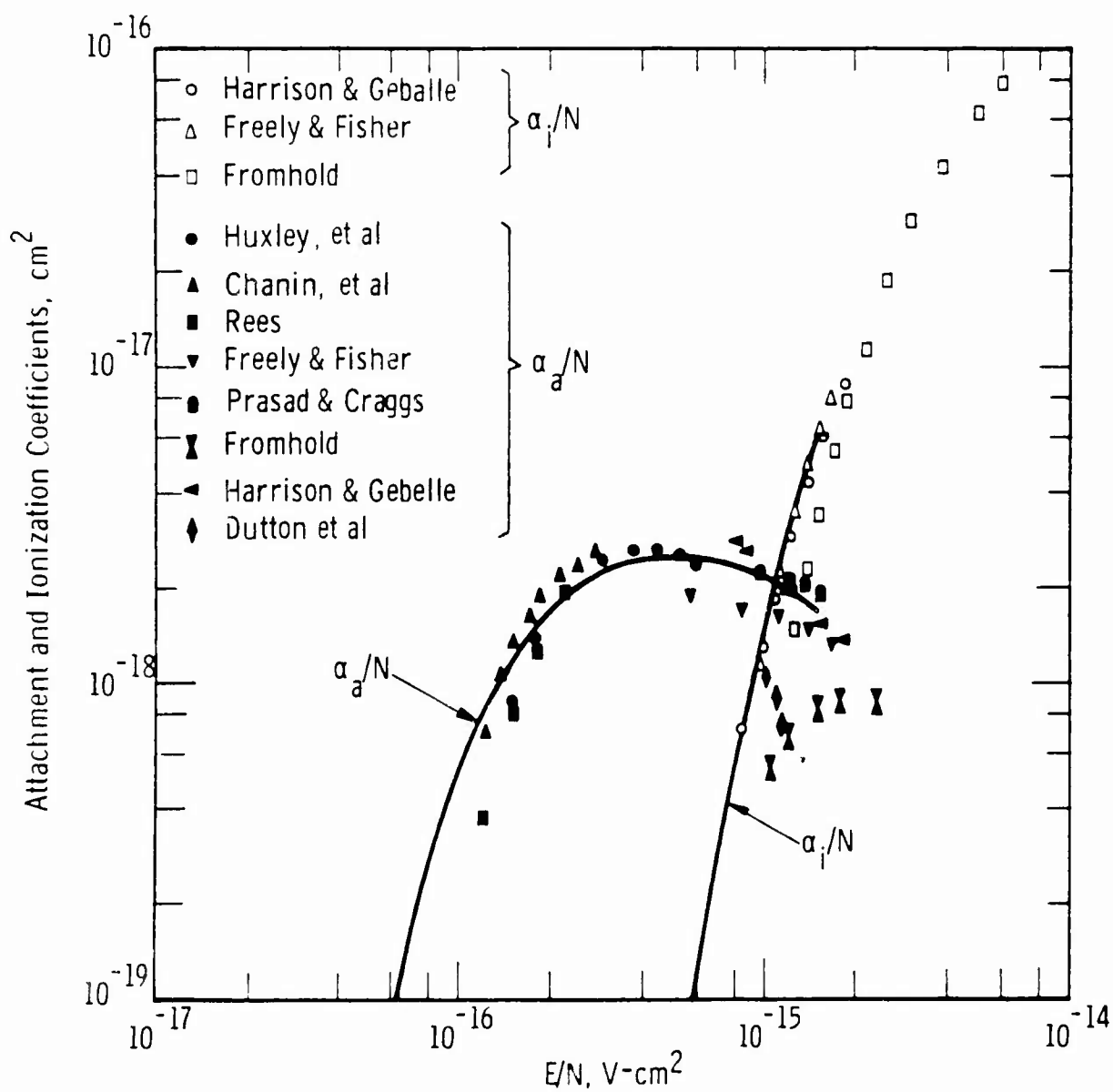
Fig. 22 Experimental and theoretical attachment and ionization
coefficients for electrons in oxygen. The solid and open points
give measured values of α_a/N and α_i/N, respectively. The curves
are the results of our calculations using the cross sections
discussed in the text.

53
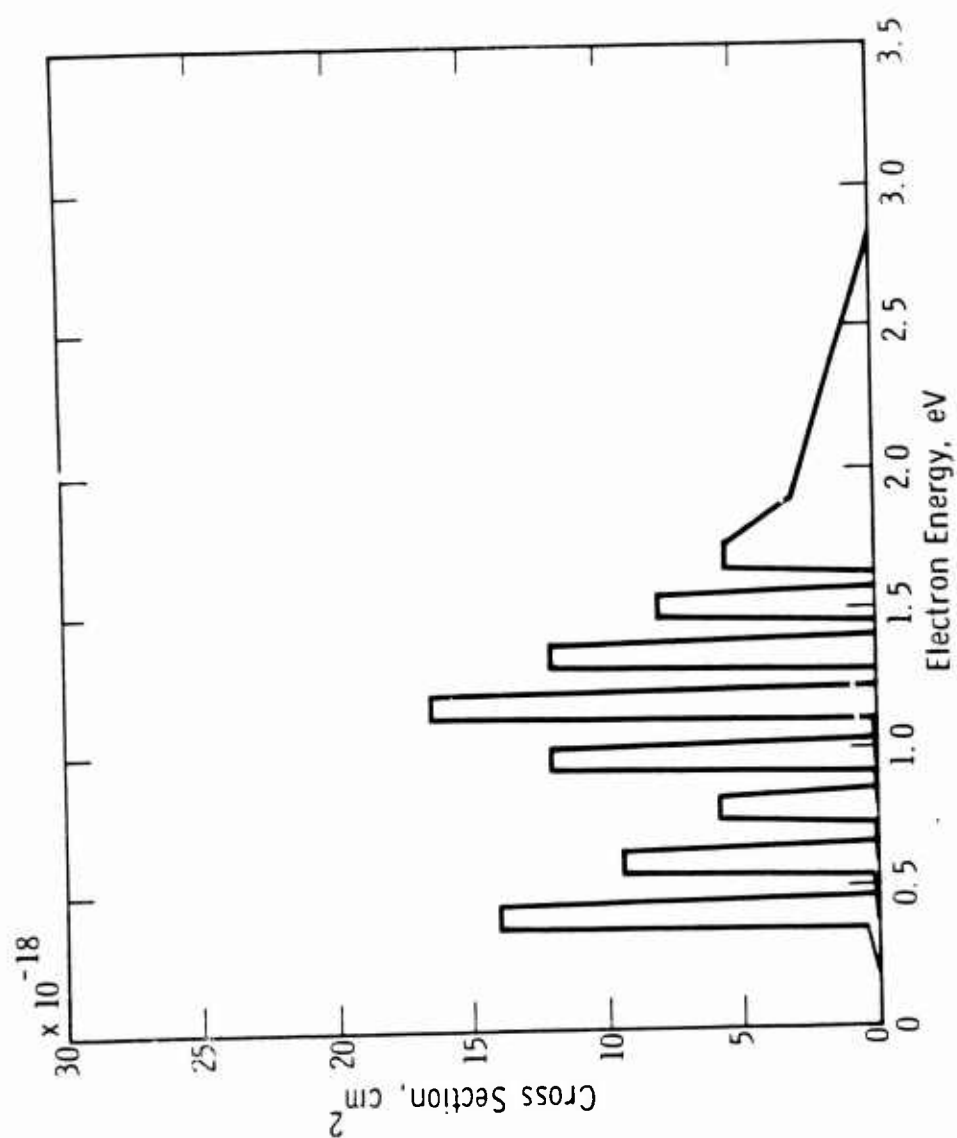
Fig. 23 Vibrational excitation cross sections derived from experimental v_u/N curve of Fig. 21.
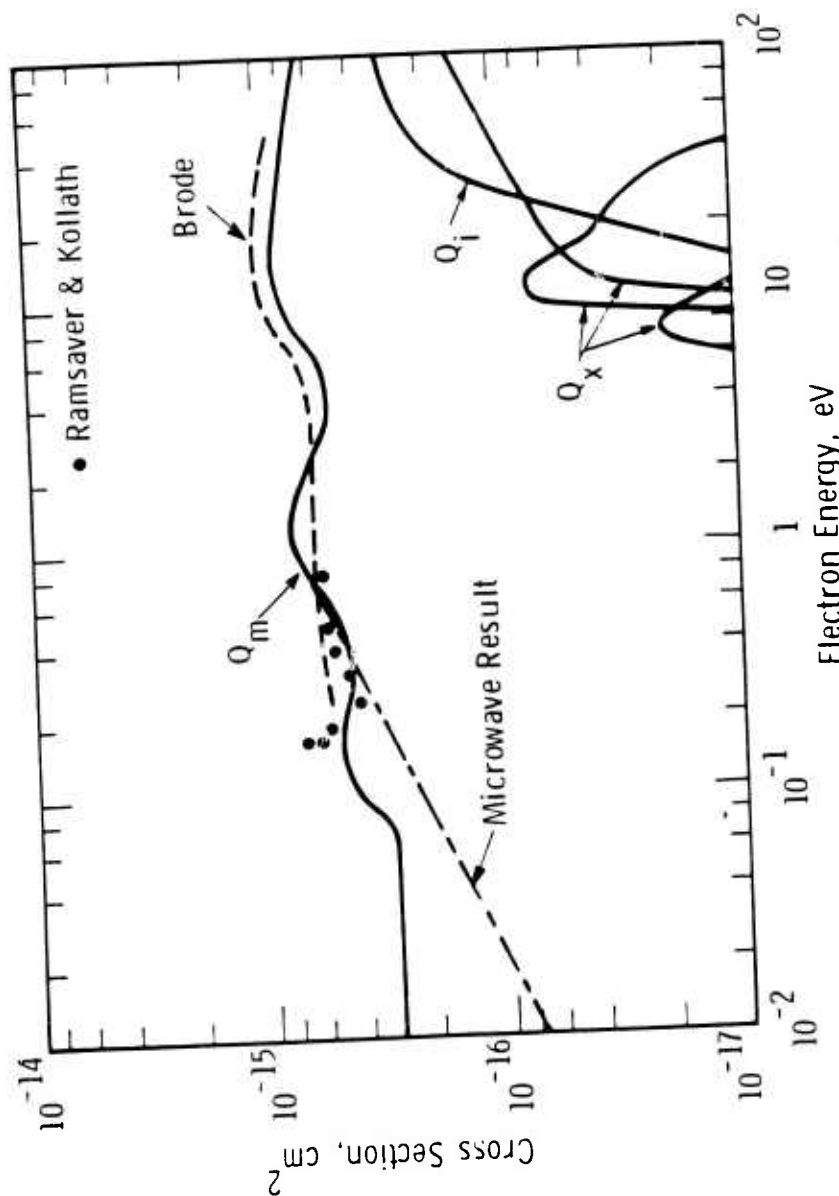
Fig. 24 Momentum transfer and inelastic cross sections derived from experimental v/N and v/N data. The ionization cross section, Q_i, is taken from Tate and Smith. The results of electron beam measurements of the total scattering cross section of Ramsauer and Kollath and of Brode are shown by the points and the dashed line. Also shown is the energy dependent momentum transfer cross section derived from microwave experiments.

55

of short lived vibrational states of the $^2\pi_g$ ground state of the O_2^- ion, then the assumptions are consistent with structure observed by Schulz[43] in the energy dependence of the three-body attachment coefficient. Although it is possible that the capture of an electron into any one of the temporary negative ion states will be followed by autodetachment and excitation of any of the energetically available vibrational states as in nitrogen,[46] we have no experimental or theoretical basis for assigning the relative magnitudes of vibrational excitation cross sections. We will, therefore, assign all of each resonant cross section to the vibrational state having its threshold just below the resonance. This is shown in Fig. 23. The derived cross sections will, therefore, be weighted sums of the true cross sections.

The widths in energy of the cross sections shown in Fig. 23 are chosen for computational convenience and only their integrated magnitudes are expected to correspond to reality, i.e., Fig. 23 is more properly interpreted as showing that the integral of the cross section over energy for the first resonant peak is approximately $1.4 \times 10^{-18} cm^2$-eV. If the magnitude of the first resonances were $\pi/k^2 = 3 \times 10^{-15} cm^2$ where k is the electron wave number then the width of the peak would be roughly 5×10^{-4} eV or the lifetime of the compound state would be 10^{-12} sec. Only the magnitudes of the resonant portions of the cross sections are adjusted during the calculations. Our assignment of all of the inelastic cross sections for electron energies between 0.9 and 4.4 eV to vibrational excitation is rather questionable in view of the possible excitation of the $a^1\Delta_g$ and $b^1\Sigma_g^+$ states. In fact, the increase in the derived cross sections for energies above 0.98 eV suggests that new modes of excitation, e.g., $a^1\Delta_g$ excitation, is important. We do not know whether the resonance type of excitation is applicable to the excitation of the $a^1\Delta_g$ and $b^1\Sigma_g^+$ levels. An additional complication which we have not taken into account is the possibility that there are resonances due to other electronic states of the negative ion, e.g., vibrational levels of the $^4\Sigma_g^-$ state of O_2^-. If we were to assume a set of resonant cross sections located at the vibrational excitation thresholds of the $X^3\Sigma_g^-$ ground state instead of the delayed resonances shown in Fig. 23, then the magnitude of the lowest energy peak would be lowered by a factor of approximately six. The decrease in

56

\

magnitude would decrease with increasing threshold energy.

The cross section for momentum transfer collisions, Q_m, for oxygen obtained from our analysis is shown in Fig. 24. When this cross section is combined with the vibrational excitation cross sections of Fig. 23 and with a set of rotational excitation cross sections calculated from the theory of Gerjuoy and Stein[47] using an effective quadrupole moment of 1.5 ea_o^2, we obtain the set of v_m/N and v_u/N values shown by the solid circles of Fig. 21 and the values of w and ϵ_k shown by the solid line of Fig. 20. Thus, we are able to obtain good agreement with an average of the experimental values of v_m/N and v_u/N shown by the solid curve of Fig. 22. The portion of the Q_m curve below 0.1 eV is chosen to give a reasonable fit to the values for the mobility of thermal electrons in O_2 obtained by Pack and Phelps[39] from measurements in O_2-CO_2 mixtures and shown in Fig. 23. However, we note that the thermal mobility inferred by Pack and Phelps[48] from equilibrium constant data would require significantly smaller values of Q_m. Similar low values of Q_m are obtained when one fits Q_m to the microwave conductivity data of van Lint, et al.,[49] Fehsenfeld,[50] of Mentzoni,[51] and of Veach, et al.,[52] for near thermal electrons in O_2. The Q_m curve derived from the microwave results of Mentzoni and of Veach, et al. is shown dashed in Fig. 24. On the other hand, the high frequency conductivity data of Carruthers[53] is consistent with values of Q_m reasonably close to the values given by the solid curve of Fig. 24. One notes that one conceivable way to make the dashed Q_m curve yield drift velocities in agreement with the non-thermal values of Fig. 20 is to assume a resonance peak section at about 0.15 eV. Evidence for such a peak was found by Ramsauer and Kollath.[54] Such a peak would have to have an integrated cross section of roughly 5×10^{-17} cm^2 eV and would be due to the compound state which is responsible for the attachment of low energy electrons [16,43] (< 0.3 eV) in the three-body process. This point needs to be investigated in detail.

The effective quadrupole moment of 1.5 ea_o^2 used to fit the drift velocity data at low E/N is to be compared with an upper limit of 0.4 ea_o^2 obtained from microwave studies of line broadening.[55] Evidence for a large effective quadrupole moment has recently been obtained by Mentzoni and Narasing Rao[56] from measurements of the decay of electron energy during

57

the afterglow of a discharge in oxygen. Very recently, Takayanagi[57] has obtained cross sections for rotational excitation in oxygen which differ greatly in shape and magnitude from those calculated using the Gerjuoy and Stein relations. We have not yet used these cross sections in our calculations.

V C. Moderate Energies $(1.0 < \epsilon_k < 3.0 \text{ eV})$

Shown in Fig. 25 are the electronic excitation and ionization cross sections used to fit the measured transport coefficients. The thresholds for the three excitation cross sections, i.e., 4.5, 8.0, and 9.7 eV were taken from Schulz and Dowell.[44] The magnitudes and energy dependence of the cross sections were adjusted to fit the v_u/N and ionization coefficient curves. As pointed out by Schulz and Dowell the apparent thresholds at 4.5 and 8.0 eV correspond to expected appearance potentials for the $A^3\Sigma_u^+$ and $B^3\Sigma_u^-$ levels, respectively. The threshold at 9.7 eV is a rather arbitrary choice from among the large amount of structure observed in the trapped electron experiments[44] at energies above about 8.5 eV.

For ϵ_k values between 0.6 and 2.5 the 4.5 eV process had a greater effect on the v_u/N curve than any other individual cross section, and from 1.0 to 2.5 eV at least half the total v_u was due to this level. Consequently we expect the rising portion of that cross section curve to be quite accurate. The falling portion of the 4.5 eV process cannot be considered too accurate because of the interaction with the 8 eV process and because of the inherent insensitivity of our technique for inelastic cross sections which decrease with increasing electron energy.

The magnitude of the process with threshold at 8.0 eV was adjusted to give a fit to the high energy portion of the v_u/N curve above 2 eV. Using Tate and Smith's[58] ionization cross section, the magnitude of the 9.7 eV process was adjusted to give a fit to the ionization coefficient α_i/N data of Harrison and Geballe,[34] Prasad and Craggs,[40] Freely and Fisher[42] shown in Fig. 22. The same result could probably have been obtained by adding a significant high-energy portion to the 8.0 eV process as suggested by the results of Lassettre, Silverman and Krasnow[59] or by adding cross sections corresponding to lower or higher thresholds. This

58
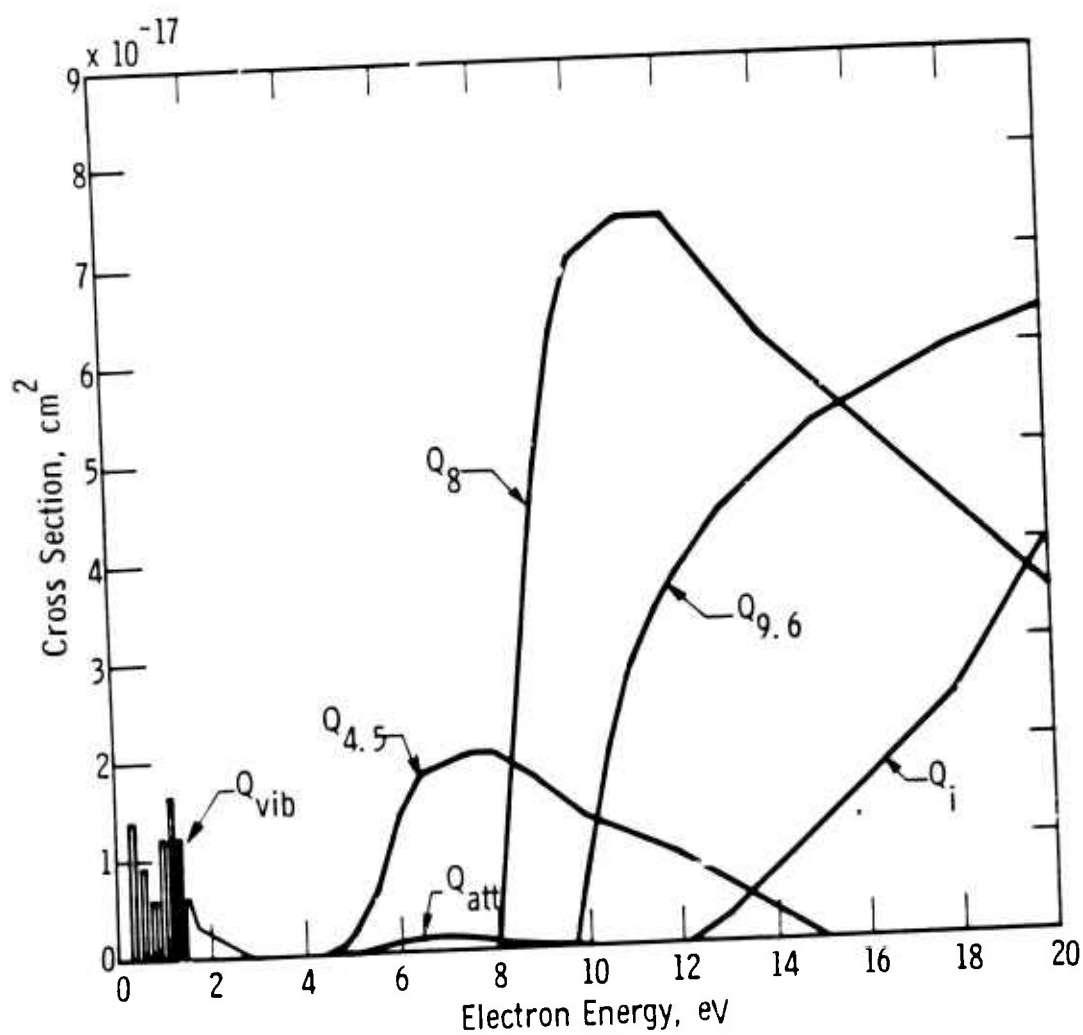
Fig. 25 Inelastic collision cross sections derived from ν_u/N, α_a/N and α_i/N data of Figs. 21 and 22 and threshold data of Schulz and Dowell. The subscripts to the Q's indicate the process involved. Thus, $Q_{4.5}$ is the excitation cross section for the $A^3\Sigma_u^+$ level with a threshold at 4.5 eV while Q_{att} is the dissociative attachment cross section from electron beam experiments.

59

illustrates that the weighted sum of our results above 8 eV should be considered more significant than the individual cross sections. If we were to attempt to fit the α_i/N data of Dutton, Llewlyn-Jones and Morgan[41] or of Fromhold[36] we would have to assume significantly larger inelastic collision cross sections. We have not attempted to fit the α_i/N and α_a/N data for $E/N > 1.5 \times 10^{-15} V\text{-}cm^2$ since for higher E/N the energy required to bring the electrons produced by ionizing collisions up to the mean electron energy can no longer be neglected and since we expect poor convergence of the spherical harmonic expansion of the electron energy distribution used in our analysis.[25,37]

In Fig. 22 we have compared our calculated attachment coefficient α_a/N with experiment. We have used the attachment cross section measured by Schulz.[60] The effect of the attachment cross section was too small to be noticeable in the v_u/N curves. We have used the comparison of calculated and experimental attachment coefficients in an effort to check on the validity of our elastic and inelastic cross sections. Except for the region below a field strength of $1.3 \times 10^{-16} V\text{-}cm^2$, the agreement is considered satisfactory. A change in the threshold of the attachment cross section from 4.4 eV to 4.9 eV produced little change in the attachment coefficient. Modifying the inelastic cross sections to provide better agreement for α_a/N at low field strengths resulted in v_u/N curves that were too high by 50% in the ϵ_k region from 1 to 2 eV. We decided to accept the disagreement in the attachment coefficient in favor of a good fit to the v_u/N curve. Resolution of this discrepancy does not appear possible at this time. At present it does not appear possible to fit the rise in α_a/N with E/N found by Fromhold and remain consistent with the attachment cross section of Schulz and others and the ϵ_k data of Huxley, Crompton and Bagot.[35] Similarly, the rapid decrease in α_a/N with E/N found by Dutton, Llewlyn-Jones, and Morgan would appear to be very difficult to fit theoretically. It presumably would not be too difficult to obtain a theoretical curve passing through the average of these two sets of data.

VI

RECOMMENDATIONS FOR FUTURE WORK

On the basis of the work presented in this report, we make the following recommendations for future investigations:

1. It is recommended that the temperature dependent studies of electron-positive ion recombination in atmospheric gases discussed in Section III be continued and where possible, extended over a wider temperature range. Some specific investigations which should be considered are, a) conformation of the observed temperature dependence of N_2^+ ion-electron recombination using the single pulse technique, b) measurement of the temperature dependent recombination coefficient for N_4^+ ions and electrons using the single pulse technique in addition to c) temperature dependent studies of electron-ion recombination in oxygen and nitric oxide. Effort should be made to study the effects of temperature on the relative concentrations of the various complex ions, such as N_3^+, N_4^+ and O_3^+, observed in the afterglow. In addition, work should be continued on the improvement of the correlation between the observed time variation of the electron density and the positive ion density (see Technical Report AFWL-TR-64-178) in the cases of O_2^+ and NO^+.

2. On the basis of the studies presented in Section IV, it is recommended that the experiments involving oxygen negative ions and mixtures of atomic and molecular oxygen be continued in order to determine the role of associative detachment in the ionosphere. The possibility of an associative detachment reaction involving excited molecular oxygen should also be investigated. Data obtained with the high pressure mass spectrometer have indicated that complex negative ions, e.g., O_3^-, CO_3^-, CO_4^-, $(H_2O) \cdot O_2^-$, etc., are readily formed under suitable conditions. It is recommended that the negative ion content of various mixtures of common atmospheric gases be investigated and that the rates of formation of the complex ions be determined wherever possible. In view of some of the data presented in Section IV, mass spectrometers to be used in rocket probes of the ionosphere should be designed to measure ions having masses up to 100 mass units.

3. It is recommended that efforts to obtain reliable values for the elastic and inelastic collision cross sections in O_2 be continued. At present the available experimental data lead to two significantly different

61

estimates for the momentum transfer cross section for thermal electrons in O_2. An effort should be made to obtain experimental data which will resolve this discrepancy. As improved experimental data become available analyses should be performed in order to determine the corresponding cross sections. An attempt should be made to obtain more direct experimental evidence for the resonant peaks which we have proposed to explain the vibrational excitation of O_2.

REFERENCES

1. W. H. Kasner and M. A. Biondi, Phys. Rev. $\underline{137}$, A317. (1965).

2. See, for example, M. H. Mentzoni, J. Geophys. Res. $\underline{68}$, 4181 (1963);
    R. Hackam, Plant. Space Sci., $\underline{13}$, 667 (1965); and E. P. Bialecke and
    A. A. Dougal, J. Geophys. Res. $\underline{63}$, 539 (1958).

3. W. H. Kasner, W. A. Rogers, and M. A. Biondi, Phys. Rev. Letters $\underline{7}$,
    321 (1961) and W. H. Kasner and M A. Biondi, Phys. Rev. $\underline{137}$, A317
    (1965). See also Air Force Weapons Laboratory Report (AFWL-TR-64-178).

4. See, for example, M. A. Biondi, Phys. Rev. $\underline{129}$, 1181 (1963), and H J.
    Oskam and V. R. Mittelstadt, Phys. Rev. $\underline{132}$, 1445 (1963). See also
    the review by M. A. Biondi in "Advances in Electronics and Electron
    Physics," edited by L. Morton (Academic Press, New York, 1963).

5. See, for example, D. R. Bates and H.S.W. Massey, Proc. Roy. Soc. (London)
    $\underline{A187}$, 261 (1946); H.S.W. Massey, "Advances in Physics," edited by
    N. F. Mott (Taylor and Francis, Ltd., London, 1952), Vol. 1, p. 395;
    T. M. Donahue, Planetary Space Sci. $\underline{13}$, 1965 (in press); and E. E.
    Ferguson, et al., J. Geophys. Res. $\underline{70}$, 4323 (1965).

6. See, for example, M. A. Biondi and S. C. Brown, Phys. Rev. $\underline{76}$, 1697
    (1949); A. C. Faire and K.S.W. Champion, Phys. Rev. $\underline{113}$, 1 (1949);
    R. B. Bryan, R. B. Holt, and O. Oldenberg, Phys. Rev. $\underline{106}$, 83 (1957);
    and M.H. Mentzoni, J. Geophys. Res. $\underline{68}$, 4181 (1963).

7. M. A. Biondi and S. C. Brown, Phys. Rev. $\underline{75}$, 1700 (1949).

8. M. A. Biondi, Rev. Sci. Instr. $\underline{22}$, 500 (1951).

9. R.L.F. Boyd and D. Morris, Proc. Phys. Soc. (London) $\underline{68}$, 1 (1955).

10. M. A. Biondi, Rev. Sci. Instr. $\underline{30}$, 831 (1959).

11. D. R. Bates and H.S.W. Massey, Proc. Phys. Soc. (London) $\underline{A187}$, 261 (1946).

12. A. V. Phelps, Tech. Rept. AFWL-TR-64-178 (1965).

13. J. E. Morgan, et al., Disc. Faraday Soc. $\underline{33}$, 118 (1962).

14. A. V. Phelps and J. L. Pack, Phys. Rev. Letters $\underline{6}$, 111 (1961).

15. F. Kaufmann, Proc. Phys. Soc. (London) $\underline{A247}$, 123 (1958).

16. L. M. Chanin, A. V. Phelps, and M. A. Biondi, Phys. Rev. $\underline{128}$, 219 (1962).

17. G. B. Kistiakowsky and G. G. Volpi, J. Chem. Phys. $\underline{28}$, 665 (1958).

18. E. C. Beaty, L. M. Branscomb, and P. L. Patterson, Bull. Am. Phys. Soc.
    $\underline{9}$, 535 (1964).

19. A. V. Phelps and J. L. Pack, 10th International Symposium on Combustion 1964, edited by The Combustion Institute, Pittsburgh, Pa., p. 569.

20. B. J. Munson and A. M. Tyndall, Proc. Roy. Soc. A172, 28 (1939).

21. R. S. Narcisi and A. D. Bailey, J. Geophys. Res. 70, 3687 (1965).

22. G. J. Schulz, J. Chem. Phys. 33, 1661 (1960).

23. E. E. Muschlitz and T. L. Bailey, J. Chem. Phys. 60, 681 (1956).

24. L. S. Frost and A. V. Phelps, Phys. Rev. 127, 1621 (1962).

25. A. G. Engelhardt and A. V. Phelps, Phys. Rev. 131, 2.15 (1963).

26. A. G. Engelhardt, A. V. Phelps and C. G. Risk, Phys. Rev. 135, A1566 (1964).

27. L. S. Frost and A. V. Phelps, Phys. Rev. 136, A1538 (1964).

28. H. L. Brose, Phil. Mag. 50, 536 (1925).

29. J. S. Townsend and V. A. Bailey, Phil. Mag. 42, 873 (1921).

30. R. A. Nielsen and N. E. Bradbury, Phys. Rev. 51, 69 (1937).

31. R. H. Healey and C. B. Kirkpatrick as given in R. H. Healey and J. W. Reed, The Behavior of Slow Electrons in Gases (Amalgamated Radio, Sydney, Australia, 1941), p. 94.

32. W. Riemann, Z. Physik 122, 216 (1944).

33. A. Doehring, Z. Naturforsch. 7, 253 (1952).

34. M. A. Harrison and R. Geballe, Phys. Rev. 91, 1 (1953).

35. L.G.H.Huxley, R. W. Crompton, and C. H. Bagot, Australian J. Phys. 12, 303 (1959).

36. L. Frommhold, Fortschritte der Physik 12, 597 (1964).

37. H. Schlumbohm, Z. Physik 184, 492 (1965).

38. J. A. Rees, Australian J. Phys. 18, 411 (1965).

39. J. L. Pack and A. V. Phelps, J. Chem. Phys. (15 February) (1966).

40. A. N. Prasad and J D. Craggs, Proc. Phys. Soc. (London) 78, 385 (1961).

41. J. Dutton, F. Llewellyn-Jones, and G. B. Morgan, Nature 198, 680 (1963).

42. J. B. Freely and L. H. Fisher, Phys. Rev. 133, A304 (1964).

43. G. J. Schulz, Bull. Am. Phys. Soc. 6, 387 (1961).

44. G. J. Schulz and J. T. Dowell, Phys. Rev. 128, 174 (1962).

45. This assumption is rather different than that used in an earlier attempt to analyze O_2 data. See A. V. Phelps, Natl. Bur. Std. Tech. Note No. 211, Vol. 5 (1964).

46. G. J. Schulz, Phys. Rev. 125, 229 (1962) and 135, A988 (1964).

47. E. Gerjuoy and S. Stein, Phys. Rev. 97, 1671 (1955) and 98, 1848 (1955).

48. J. L. Pack and A. V. Phelps, J. Chem. Phys. to be submitted (1966).

49. V.A.J. van Lint, E. G. Wikner, and D. L. Trueblood, Bull. Amer. Phys. Soc. 5, 122 (1960). See also General Atomic Division of General Dynamics Corp. Report GACD-2461 (1961) San Diego, California (unpublished).

50. F. C. Fehsenfeld, J. Chem. Phys. 39, 1653 (1963).

51. M. H. Mentzoni, J. Research Natl. Bur. Standards 69D, 213 (1965).

52. G. E. Veatch, J. T. Verdeyen, and J. H. Cahn, Paper B7, 18th Gaseous Electronics Conference, Minneapolis, October 1965.

53. J. A. Carruthers, Canad. J. Phys. 40, 1528 (1962).

54. C. Ramsauer and R. Kollath, Z. Physik 4, 91 (1930).

55. W. V. Smith and R. Howard, Phys. Rev. 79, 132 (1950).

56. M. H. Mentzoni and K. V. Narasinga Rao, Phys. Rev. Letters 14, 779 (1965).

57. K. Takayanagi, Report of Ionosphere and Space Research Japan 19, 1 (1965). See also S. Geltman and K. Takayanagi, Phys. Rev. submitted (1965) and Y. D. Oksyuk, J. Exptl. Theoret. Phys. (USSR) 49, 1261 (1965).

58. J. T. Tate and P. T. Smith, Phys. Rev. 39, 270 (1932).

59. E. N. Lassettre, S. M. Silverman and M. E. Krasnow, J. Chem. Phys. 40, 1261 (1964).

60. G. J. Schulz, Phys. Rev. 128, 178 (1962).

DISTRIBUTION

<u>No. cys</u>

HEADQUARTERS USAF

Hq USAF, Wash, DC

1   (AFRNE-B)

1   (AFTAC)

1 USAF Dep, The Inspector General (AFIDI), Norton AFB, Calif 92409

1 USAF Directorate of Nuclear Safety (AFINS), Kirtland AFB, NM 87117

MAJOR AIR COMMANDS

1 AFSC (SCT), Andrews AFB, Wash, DC 20331

1 AUL, Maxwell AFB, Ala 36112

AFSC ORGANIZATIONS

1 RTD (RTS), Bolling AFB, Wash, DC 20332

1 AF Msl Dev Cen (RRRT), Holloman AFB, NM 88330

1 AEDC (AEYD/Capt T.L. Hershey), Arnold AFS, Tenn 37289

KIRTLAND AFB ORGANIZATIONS

1 AFSWC (SWEH), Kirtland AFB, NM 87117

  AFWL, Kirtland AFB, NM 87117

20   (WLIL)

1   (WLR)

5   (WLRT)

OTHER AIR FORCE AGENCIES

Director, USAF Project RAND, via: Air Force Liaison Office, The RAND Corporation, 1700 Main Street, Santa Monica, Calif 90406

1   (RAND Physics Div)

1   (RAND Library)

1   (Dr. F. Gilmore)

1   (Dr. R. Lelevier)

1   (Dr. C. Crain)

1 AFCRL (ATTN: Dr. K. Champion/Photo Chemistry Lab), L.G. Hanscom Fld, Bedford, Mass 01731

ARMY ACTIVITIES

1 Chief of Research and Development, Department of the Army (Scientific and Technical Information Division, CRD/P), Wash, DC 20310

DISTRIBUTION (cont'd)

No. cys

1 Director, Ballistic Research Laboratories (Library), Aberdeen Proving Ground, Md 21005

1 Commanding Officer, Picatinny Arsenal (SMUPA-TN, Nike X Engineering Division), Dover, NJ 07801

1 Director, US Army Waterways Experiment Sta (WESRL), P.O. Box 631, Vicksburg, Miss 39181

NAVY ACTIVITIES

1 Commanding Officer, Naval Research Laboratory, Wash, DC 20390

1 Commander, Naval Ordnance Laboratory, ATTN: Dr. Rudlin, White Oak, Silver Spring, Md 20910

1 Office of Naval Research, Wash, DC 20360

1 Commanding Officer, US Naval Weapons Evaluation Facility (NWEF, Code 404), Kirtland AFB, NM 87117

OTHER DOD ACTIVITIES

Director, Defense Atomic Support Agency, Wash, DC 20301

2 (Document Library Branch)

1 (DASARA-2/Dr. C. Blank)

1 Director, Advanced Research Projects Agency, Department of Defense, The Pentagon, Wash, DC 20301

20 DDC (TIAAS), Cameron Station, Alexandria, Va 22314

OTHER

Massachusetts Institute of Technology, Lincoln Laboratory, P.O. Box 73, Lexington, Mass 02173

1 (Document Library)

1 (Dr. J. Pannell)

General Atomic Division, General Dynamics Corporation, 10955 John Jay Hopkins Drive, San Diego, Calif 92121

1 (ATTN: G.L. Layton)

1 (ATTN: Dr. V. Van Lint)

General Electric Company, MSD, P.O. Box 8555, Philadelphia 1, Pa.

1 (ATTN: Dr. F.A. Lucy, Room M9505)

1 (ATTN: Dr. Bortner/Aerophysics Operation)

1 (ATTN: Dr. Baulknight/Aerophysics Operation)

DISTRIBUTION (cont'd)

No. cys

General Electric TEMPO, 735 State Street, Santa Barbara, Calif

1   (Dr. R. W. Hendrick)

1   (Dr. R. Christian)

1   (Dr. W. Dudziak)

1   National Bureau of Standards, ATTN: Dr. L. M. Branscomb, Boulder, Colo

Stanford Research Institute, Menlo Park, Calif 94025

1   (Dr. C. Cock)

1   (G-037, External Reports)

Aeronutronic, Division of Ford Motor Company, Ford Road, Newport Beach, Calif

1   (Dr. Ernest Bauer)

1   (Dr. A. Katz)

1   (Dr. A. Ruhlig)

Lockheed Missile and Space Company, 3251 Hanover Street, Palo Alto, Calif

1   (Dr. R. Meyerott)

1   (Dr. D. Holland)

1   (Dr. R. Landshoff)

1   (Dr. R. Gunton)

1   Cornell Aeronautic Laboratories, ATTN: Dr. D. Malone, Buffalo, NY

Geophysics Corporation of America, Bedford, Mass

1   (Mr. George Victor)

1   (Dr. Gordon Webb)

1   (Dr. A. Dalgarno)

1   New York University, ATTN: Dr. S. Borowitz, Institute of Mathematical Sciences, New York, NY

1   Edgerton, Germeshausen, and Grier, Inc., ATTN: Dr. M. Schuler, 1660 Brookline Avenue, Boston 15, Mass

1   IIT Research Institute, ATTN: Dr. C. Haaland, 10 West 35th St, Chicago, Ill

1   Kaman Aircraft Corp, Nuclear Div, ATTN: Dr. F. Shelton, Garden of the Gods Road, Colorado Springs, Colo

1   Convair Division of General Dynamics, ATTN: Dr. D. Hamlin, 3165 Pacific Highway, San Diego, Calif

1   University of Washington, ATTN: Dr. R. R. Geballe, Seattle 5, Wash

1   G. C. Dewey Corporation, ATTN: Dr. R. Ruffine, 202 East 44th St, New York 17, NY

DISTRIBUTION (cont'd)

No. cys

University of Pittsburgh, Pittsburgh, Pa

1   (Dr. M. A. Biondi)

1   (Dr. W. L. Fite)

1   General Dynamics/Astronautics, ATTN: Dr. Magnuson, 3165 Pacific Highway, San Diego 12, Calif

10   Westinghouse, ATTN: Dr. A. V. Phelps, Beulah Road, Churchill Borough, Pittsburgh, Pa

1   Clearinghouse, ATTN: 410.11, 5285 Port Royal Road, Springfield, Va 22151

1   Official Record Copy (WLRT/Capt Sparks)

This page intentionally left blank.

DOCUMENT CONTROL DATA - R&D

(Security classification of title, body of abstract and indexing annotation must be entered when the overall report is classified)

1. ORIGINATING ACTIVITY *(Corporate author)*	2a. REPORT SECURITY CLASSIFICATION
Westinghouse Research Laboratories Pittsburgh, Pennsylvania	Unclassified
	2b. GROUP

3. REPORT TITLE

STUDIES AND EXPERIMENTAL WORK ON ATOMIC COLLISION PROCESSES OCCURRING IN ATMOSPHERIC GASES

4. DESCRIPTIVE NOTES *(Type of report and inclusive dates)*

22 December 1964 to 22 December 1965

5. AUTHOR(S) *(Last name, first name, initial)*

Phelps, A. V.; Kasner, W. H.

6. REPORT DATE	7a. TOTAL NO. OF PAGES	7b. NO. OF REFS
May 1966	76	60

8a. CONTRACT OR GRANT NO.	9a. ORIGINATOR'S REPORT NUMBER(S)
AF29(601)-6729 b. PROJECT NO. 5710	AFWL-TR-66-34
c. Subtask No. 07.010	9b. OTHER REPORT NO(S) *(Any other numbers that may be assigned this report)* Research Report 66-6E2-GASES-R1, Westinghouse Proprietary Class 3.
d.	

10. AVAILABILITY/LIMITATION NOTICES

Distribution of this document is unlimited.

11. SUPPLEMENTARY NOTES	12. SPONSORING MILITARY ACTIVITY
	Air Force Weapons Laboratory (WLRT) Kirtland Air Force Base, New Mexico 87117

13. ABSTRACT

Temperature dependent recombination studies in nitrogen have been conducted over the range 200-480°K, yielding a coefficient of $(2.9 \pm 0.3) \times 10^{-7} cm^3/sec$ for the recombination of N_2+ ions and electrons. The observed temperature dependence is quite small, being adequately described by the relation $T^{-0.02}$. Several modifications have been made on the flow system used in the study of associative detachment in O_2-O mixtures. In subsequent studies a reaction resembling associative detachment has been observed. While preliminary tests were being conducted on the rf mass spectrometer which is to be used on the flow system, a brief study of negative ion-molecule reactions was made. Rate coefficients for several of these reactions were measured. A summary of the results of a calculation of momentum transfer and inelastic cross sections for electrons in oxygen is presented. The computed momentum transfer cross section is in satisfactory agreement with electron beam results but it differs significantly from the cross section obtained at thermal energies from microwave experiments.

DD FORM 1 JAN 64 **1473**

14.		LINK A		LINK B		LINK C	
KEY WORDS		ROLE	WT	ROLE	WT	ROLE	WT
Atomic collisions							
Recombination processes							
Attachment and detachment processes							
Inelastic cross sections							
Momentum transfer							

INSTRUCTIONS

1. ORIGINATING ACTIVITY: Enter the name and address of the contractor, subcontractor, grantee, Department of Defense activity or other organization (*corporate author*) issuing the report.

2a. REPORT SECURITY CLASSIFICATION: Enter the overall security classification of the report. Indicate whether "Restricted Data" is included. Marking is to be in accordance with appropriate security regulations.

2b. GROUP: Automatic downgrading is specified in DoD Directive 5200.10 and Armed Forces Industrial Manual. Enter the group number. Also, when applicable, show that optional markings have been used for Group 3 and Group 4 as authorized.

3. REPORT TITLE: Enter the complete report title in all capital letters. Titles in all cases should be unclassified. If a meaningful title cannot be selected without classification, show title classification in all capitals in parenthesis immediately following the title.

4. DESCRIPTIVE NOTES: If appropriate, enter the type of report, e.g., interim, progress, summary, annual, or final. Give the inclusive dates when a specific reporting period is covered.

5. AUTHOR(S): Enter the name(s) of author(s) as shown on or in the report. Enter last name, first name, middle initial. If military, show rank and branch of service. The name of the principal author is an absolute minimum requirement.

6. REPORT DATE: Enter the date of the report as day, month, year; or month, year. If more than one date appears on the report, use date of publication.

7a. TOTAL NUMBER OF PAGES: The total page count should follow normal pagination procedures, i.e., enter the number of pages containing information.

7b. NUMBER OF REFERENCES: Enter the total number of references cited in the report.

8a. CONTRACT OR GRANT NUMBER: If appropriate, enter the applicable number of the contract or grant under which the report was written.

8b, 8c, & 8d. PROJECT NUMBER: Enter the appropriate military department identification, such as project number, subproject number, system numbers, task number, etc.

9a. ORIGINATOR'S REPORT NUMBER(S): Enter the official report number by which the document will be identified and controlled by the originating activity. This number must be unique to this report.

9b. OTHER REPORT NUMBER(S): If the report has been assigned any other report numbers (*either by the originator or by the sponsor*), also enter this number(s).

10. AVAILABILITY/LIMITATION NOTICES: Enter any limitations on further dissemination of the report, other than those

imposed by security classification, using standard statements such as:

(1) "Qualified requesters may obtain copies of this report from DDC."

(2) "Foreign announcement and dissemination of this report by DDC is not authorized."

(3) "U. S. Government agencies may obtain copies of this report directly from DDC. Other qualified DDC users shall request through

_____ ."

(4) "U. S. military agencies may obtain copies of this report directly from DDC. Other qualified users shall request through

_____ ."

(5) "All distribution of this report is controlled. Qualified DDC users shall request through

_____ ."

If the report has been furnished to the Office of Technical Services, Department of Commerce, for sale to the public, indicate this fact and enter the price, if known.

11. SUPPLEMENTARY NOTES: Use for additional explanatory notes.

12. SPONSORING MILITARY ACTIVITY: Enter the name of the departmental project office or laboratory sponsoring (*paying for*) the research and development. Include address.

13. ABSTRACT: Enter an abstract giving a brief and factual summary of the document indicative of the report, even though it may also appear elsewhere in the body of the technical report. If additional space is required, a continuation sheet shall be attached.

It is highly desirable that the abstract of classified reports be unclassified. Each paragraph of the abstract shall end with an indication of the military security classification of the information in the paragraph, represented as (TS), (S), (C), or (U).

There is no limitation on the length of the abstract. However, the suggested length is from 150 to 225 words.

14. KEY WORDS: Key words are technically meaningful terms or short phrases that characterize a report and may be used as index entries for cataloging the report. Key words must be selected so that no security classification is required. Identifiers, such as equipment model designation, trade name, military project code name, geographic location, may be used as key words but will be followed by an indication of technical context. The assignment of links, rules, and weights is optional.

GPO 886-551